nature biomedical engineering

ARTICLES

https://doi.org/10.1038/s41551-021-00706-z

Check for updates

Discrimination of single-point mutations in unamplified genomic DNA via Cas9 immobilized on a graphene field-effect transistor

Sarah Balderston[1,2], Jeffrey J. Taulbee[3], Elizabeth Celaya[2], Kandace Fung[1], Amanda Jiao[2], Kasey Smith[1], Reza Hajian[1,2], Giedrius Gasiunas[4,5], Simonas Kutanovas[4], Daehwan Kim[6], Jonathan Parkinson[2], Kenneth Dickerson[2], Juan-José Ripoll[2], Regis Peytavi[2], Hsiang-Wei Lu[1,2], Francie Barron[2], Brett R. Goldsmith[2], Philip G. Collins[3], Irina M. Conboy[6], Virginijus Siksnys[4,5] and Kiana Aran[1,2,6] ✉

Simple and fast methods for the detection of target genes with single-nucleotide specificity could open up genetic research and diagnostics beyond laboratory settings. We recently reported a biosensor for the electronic detection of unamplified target genes using liquid-gated graphene field-effect transistors employing an RNA-guided catalytically deactivated CRISPR-associated protein 9 (Cas9) anchored to a graphene monolayer. Here, using unamplified genomic samples from patients and by measuring multiple types of electrical response, we show that the biosensors can discriminate within one hour between wild-type and homozygous mutant alleles differing by a single nucleotide. We also show that biosensors using a guide RNA–Cas9 orthologue complex targeting genes within the protospacer-adjacent motif discriminated between homozygous and heterozygous DNA samples from patients with sickle cell disease, and that the biosensors can also be used to rapidly screen for guide RNA–Cas9 complexes that maximize gene-targeting efficiency.

Single-nucleotide polymorphisms (SNPs) account for over 50% of disease-causing mutations in humans[1–3]. In addition to residing at the core of human health genetics, SNPs play a considerable role in infectious disease prevention[4–6], ageing[7], pharmacology[8–10] and agriculture[11] and are a driving force in evolutionary change. Specific SNPs have been associated with reducing the rubella vaccine's effectiveness by impinging on key cytokine pathways[12,13]. SNPs were also implicated in an outbreak of coronavirus, causing severe acute respiratory syndrome (SARS)[14–16]. It was discovered that the virus was replicating in populations of palm civets in China[17,18], and sequencing of the gene transcribing the spike protein (that is, the protein necessary for the virus infection of host cells) revealed 27 nucleotide variations, which were indicative of the virus's new ability to infect humans[18]. A correlation between the hallmarks of human ageing and three SNPs in the circadian rhythm *CLOCK* gene has also been reported[7]. Furthermore, SNPs resulting in amino acid variations in proteins, which interact with a mutant protein, may affect a patient's prognosis, as exemplified in cystic fibrosis[19]. In drug metabolism, SNPs are particularly important for personalizing pharmaceutical therapy as they can serve as markers for a patient's metabolic capacity for a specific drug[20]. One example of this is two concomitant SNPs in two cytochrome p450 (*CYP*) genes that have been implicated in paediatric drug-resistant epilepsy[21]. In the agriculture industry, it is crucial for crop yield to plant seeds with the highest possible resistance to common pathogens. SNPs play an essential role in determining breeding procedures as they serve as markers for resistance screening[22–24]. Furthermore, SNPs can be used as genome stability markers for quality control of genetically modified seeds before their release[25]. Although the applications for SNP detection are abundant across many research disciplines and industries, current methods for SNP genotyping have limited their widespread employment outside of a traditional laboratory.

The current gold standards for massive SNP genotyping involve SNP microarrays, TaqMan SNP genotyping or next-generation sequencing[26–30]. Although many of these technologies are high throughput and have allowed for advancement in research and industry, they all require DNA amplification, experienced technical staff, tedious design of paired primer systems, and fluorescent probes, all of which are not amenable with mass testing at the point of care or in the field. Furthermore, all of these methods require sophisticated optical equipment, which restricts the capability of laboratories for DNA sequence determination, thus severely limiting the ability to design hand-held, rapid, point-of-testing instrumentation. Amplification-free electronic detection of a target gene with SNP specificity has the potential to streamline this process, allowing for mass testing for SNPs outside of a traditional laboratory.

We have previously reported on a label-free technology based on a graphene field-effect transistor (gFET) that is capable of discriminating between target and non-target genes from unamplified genomic DNA samples[31]. Here, we report a new CRISPR-based gFET system, termed CRISPR-SNP-Chip, referred to as SNP-Chip hereafter, which is capable of detecting single-nucleotide mutations in a given DNA sequence without the need for target amplification. This was accomplished by: (1) expanding the types of electrical measurements taken; and (2) incorporating different Cas9 variants

[1]Keck Graduate Institute, The Claremont Colleges, Claremont, CA, USA. [2]Cardea, San Diego, CA, USA. [3]University of California, Irvine, Irvine, CA, USA. [4]CasZyme, Vilnius, Lithuania. [5]Institute of Biotechnology, Life Sciences Center, Vilnius University, Vilnius, Lithuania. [6]University of California, Berkeley, Berkeley, CA, USA. ✉e-mail: karan@kgi.edu

and orthologues to improve SNP discrimination. In this work, we record I, C and V responses to be able to detect SNPs. This expansion of measurement type has allowed us to reach single-nucleotide specificity. Furthermore, the incorporation of a novel Cas9 orthologue has allowed us to distinguish between samples with different zygosity of a particular SNP. SNP-Chip consists of a liquid-gated gFET where the graphene channel between the source and drain electrodes is functionalized with a CRISPR-associated (Cas) enzyme complexed with a target-specific guide RNA (gRNA) to capture a specific DNA sequence contained within unamplified genomic DNA[28–30]. Electrical measurements are obtained by sweeping the liquid gate voltage from −100 mV to +100 mV while the source–drain current is measured continuously at constant source–drain voltage. Molecular adsorption and electrostatic interactions at the graphene surface create local potentials that effectively gate and alter gFET electrical properties, such as conductance, source–drain current, transconductance and the effective gate potential seen by the graphene channel. As a result, the interaction between the RNA-guided Cas nuclease and its DNA target is detectable as a change in one or more of these gFET properties, which are measured simultaneously and in real time.

The sensitivity and specificity of SNP-Chip depend on the DNA-targeting capability of Cas enzymes anchored to the graphene channel. Cas9, the most widely used Cas enzyme, is complexed with a gRNA molecule with a spacer of ~20 nucleotides complementary to a specific DNA sequence[32,33]. This complex interacts with DNA by recognizing protospacer-adjacent motifs (PAMs). When the RNA-guided Cas9 interacts with its PAM, it begins to unwind the DNA upstream of the PAM, and hybridization between the spacer sequence of the gRNA and the DNA target occurs, followed by cleavage of the DNA strand. In the absence of complementarity between the spacer and the DNA, the DNA is more likely to dissociate from the Cas9–gRNA complex[34,35].

We previously reported a DNA sequence-detecting device that used dCas9, a dead variant of Cas9 that is nuclease inactive[31,36,37]. Except for DNA cleavage, this general mechanism is consistent between dCas9 and Cas9 (refs. [32–34]). Studies have shown that Cas9 remains bound to its target DNA after cleavage[38]. Therefore, the nuclease-active wild-type Cas9 and high-fidelity Cas9 enzymes can also be used within the SNP-Chip construct to detect a specific DNA sequence. Incorporating different Cas enzymes can improve this technology's performance by tuning the SNP-Chip specificity and selectivity[39–43]. For example, high-fidelity Cas9 has been reported to mediate highly specific correction of the sickle cell disease (SCD)-associated SNP mutation in haematopoietic stem and progenitor cells of patients with SCD[44].

SNP-Chip was constructed by expanding the electronic analysis of the gFET and utilizing dCas9, Cas9 or a Cas9 orthologue to enable amplification-free electronic detection of point mutations. These studies indicated that the accuracy and SNP discrimination efficiency of Cas enzymes could be captured by accurate analysis of the gFET electrical responses. In the present study, we utilized these Cas enzymes to detect SNPs in target genes in two human disease models. In the first disease model, we tested an SCD-associated point mutation in the *HBB* gene of patients with and without the disease. SCD is a recessive heritable disease caused by an adenine to thymine base substitution within exon 1 of the *HBB* gene[45], resulting in a glutamate to valine amino acid switch in β-globin (E6V). This mutation renders β-globin prone to polymerization, causing the characteristic misshapen sickle red blood cells (RBCs)[46,47]. Sickle RBCs damage blood vessels and cause blockages, resulting in symptoms such as chronic pain, swelling, organ damage and stroke. Furthermore, patients often suffer from chronic anaemia due to the shortened lifespan of sickle RBCs[48]. These complications result in a reduction of life expectancy for patients with SCD by approximately 30 years[49,50]. Despite the associated decrease in quality of life and life expectancy, the sickle RBC trait (mutant haemoglobin S (HbS)) has persisted, particularly in malaria-endemic regions of the world such as East Africa[51]. We also tested amyotrophic lateral sclerosis (ALS) as an additional disease model by detecting a SNP in the *superoxide dismutase type 1* (*SOD1*) gene in genomic DNA extracted from human induced pluripotent stem cells (hiPSCs) from a healthy individual and an individual with familial ALS (fALS). ALS is a neurodegenerative disease characterized by the progressive loss of motor neurons in the cortex and spinal cord. This degeneration leads to death due to respiratory failure within 3–5 years[52]. Approximately 90% of all ALS cases are sporadic, occurring randomly without known specific causes and genetic background. However, about 10% of cases are hereditary and familial and are caused by single-gene mutations[53]. fALS is deeply associated with *SOD1* missense mutants such as A4V (where alanine is switched to valine at codon 4), A89V (where alanine is switched to valine at codon 89), H44R (where histidine is switched to arginine at codon 44) and G93A (where glycine is switched to alanine at codon 93). Any of these mutations may trigger a toxic mechanism involving redox catalysis, which results in misfolding of the SOD1 protein[54,55].

Recently, CRISPR-based gene editing has been utilized for the potential treatment of both SCD and ALS[56–60]. Although promising, CRISPR-based gene editing requires careful assessment of CRISPR complex design and editing efficiency[61,62]. Therefore, technologies that can detect, quantify and discriminate between different wild-type and mutated gene targets in a facile and high-throughput manner can be essential in designing better CRISPR complexes with optimal efficiency to improve the effectiveness of ex vivo genome editing in cell populations before they are reintroduced to a patient's body[57,63].

In recent years, technologies have been developed for SNP genotyping to bypass the need for advanced sequencing techniques. Although some of these technologies have removed the need for expensive and bulky optical equipment[64] and have bypassed the need for amplification[65], none have done both. SNP-Chip is a CRISPR-powered transistor capable of amplification-free detection of target DNA sequences with SNP specificity by combining the power of CRISPR and gFET technology, overcoming the limitations associated with other amplification and optical-based SNP genotyping methods. SNP-Chip is a flexible, label-free technology that can easily be reconfigured through the programmability of CRISPR to target other point mutations, broadening SNP-Chip's potential applications beyond SCD and ALS.

Results

SNP-Chip consists of a gFET fabricated using a commercial microelectromechanical system foundry, as previously described[66]. SNP-Chip uses a reader and a cartridge connected to a computer and analysis software (Fig. 1)[31,66–68]. The graphene channel, between the source and drain electrodes, is decorated with Cas enzymes via a chemical linker, 1-pyrenebutanoic acid (PBA). The chemical linker, which π–π stacks with the graphene, is chemically activated via standard carbodiimide chemistry to covalently attach the Cas enzyme to the graphene surface[31,69]. Once the enzyme is immobilized, the graphene surface is passivated with poly(ethylene glycol) (PEG) amine and ethanolamine[31,70]. The Cas enzyme immobilized on the channel forms a complex with a gRNA, which is designed to: (1) bind to the Cas enzymes; and (2) target the DNA locus containing either the SCD-associated SNP or the ALS-associated SNP. The fully functionalized SNP-Chip is calibrated, then unamplified DNA samples are incubated atop the graphene surface during continuous data acquisition (Supplementary Fig. 1). The Cas–gRNA complex interacts with the different PAMs contained within the DNA via three-dimensional diffusion[38,71,72]. In the presence of the target-adjacent PAM, complete hybridization can occur, leaving the DNA containing the complementary sequence anchored to the

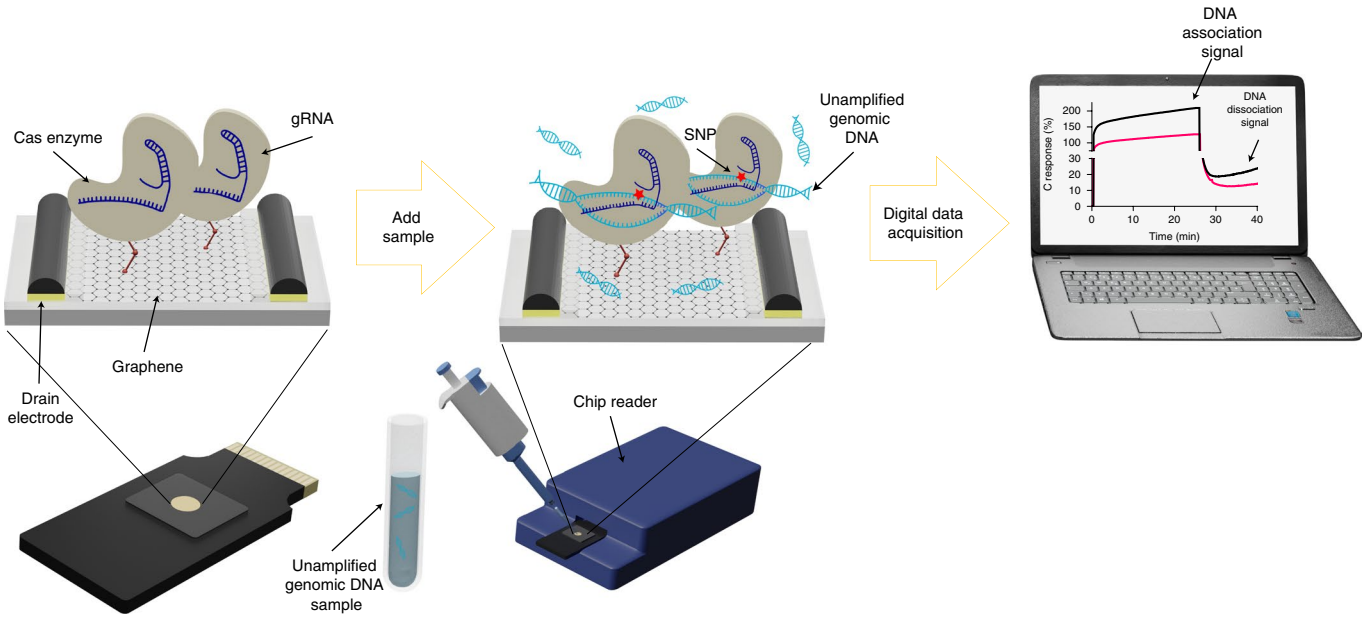

Fig. 1 | CRISPR-powered gFET for amplification-free detection of single-nucleotide mutations. SNP-Chip, the next generation of CRISPR-powered gFET, with expanded monitoring of multiple electronic parameters, can detect single-nucleotide differences within unamplified DNA samples. Through the CRISPR–Cas9 ribonucleic protein complex on its surface, this technology can digitally detect SNPs without labels or amplification. The target-specific gRNA is designed to target single-nucleotide mutations relevant to two human disease models: SCD and ALS. Through real-time, multi-parameter and digital data acquisition, SNP-Chip can discriminate between unamplified genomic DNA samples in 40 min.

surface of the graphene via the Cas–gRNA complex. In the case of DNA targets containing mismatches, the Cas–gRNA complex has less affinity for the DNA and the DNA will dissociate from the surface of the graphene altogether[35,71,73]. After incubating the DNA atop the graphene channel, the gFET is rinsed to remove non-specifically bound DNA from the graphene surface, allowing for the final signal read-out. A schematic demonstrating this workflow is shown in Fig. 1.

The SNP specificity of SNP-Chip depends on the highly specific recognition of target sequences by the Cas–gRNA complex, which requires thoughtful gRNA design. The DNA, unwound by the Cas enzyme, is probed by the gRNA spacer sequence upstream of the PAM, starting at the 3′ end of the spacer[38,74]. It is within the first few nucleotides in the so-called seed sequence where Cas9 and dCas9 are most severely affected by mismatches. It has been observed that incomplete hybridization between Cas9–gRNA complexes and DNA within the spacer seed region often results in the dissociation of Cas9 from DNA altogether[71,73]. In fact, single nucleotides within the seed region of the gRNA, although having little impact on the DNA association, have been shown to increase the rate of DNA dissociation, from $<0.006\,s^{-1}$ to $>2\,s^{-1}$ (ref. [71]). Therefore, gRNA designs used for SNP-Chip analysis that distinguish between target and non-target DNA within the PAM or the seed sequence exhibit a high degree of specificity[71] because SNP-Chip can measure the DNA dissociation signals in addition to the association signals (Fig. 1).

To study the single-nucleotide sensitivity of SNP-Chip to detect mutation in the *HBB* gene, we first obtained DNA extracts from a healthy patient (denoted HbAA) who was homozygous for the wild-type HbA *HBB* allele and a patient with SCD (denoted HbSS), who was homozygous for the sickle cell allele (E6V mutation), termed the HbS. All clinical SCD-associated DNA extracts were obtained from commercially available B lymphocyte cells (Coriell Institute). SNP-Chip was functionalized with CRISPR complexes as described above. The primary gRNA design employed in this study has previously been validated for targeting and cleavage of the *HBB* gene using Cas9 (ref. [75]). This design was selected to maximize the difference in the affinity of the interactions that occur between the HbA and HbS alleles. This gRNA targets the HbA allele, which is adjacent to a 5′-AGG-3′ PAM. This healthy targeting gRNA, compatible with Cas9 and dCas9, is denoted gRNA-HTYa hereafter. The SCD-associated SNP is the second nucleotide on the PAM-proximal end of the spacer, well within the seed sequence (Fig. 2a). A second gRNA was designed to target the same protospacer sequence for the HbS allele. This gRNA, compatible with Cas9 and dCas9, termed gRNA-SCDa, was used as a control for the amplicon SNP-Chip studies to ensure SNP-Chip specificity. Before SNP-Chip analysis, HbAA and HbSS genomic DNA samples were sequenced to: (1) confirm the absence or presence of the SCD-associated SNP in HbAA or HbSS samples; and (2) verify that the two protospacer sequences were present in the clinical DNA samples. To do this, we amplified a 504-base pair (bp) region of the *HBB* gene, encompassing all of exon 1, from both HbAA and HbSS DNA (Fig. 2b). The sequencing results shown in Fig. 2c indicate that the gRNA-HTYa and gRNA-SCDa protospacer sequences were found in HbAA and HbSS DNA, respectively, with the SCD-associated SNP present in the HbSS sample. Both sequences were directly adjacent to the Cas9 and dCas9 PAM sequence (5′-AGG-3′)[36,74].

To assess the capacity of SNP-Chip to discriminate between samples that differ by a single nucleotide, we first tested the assay with the HbAA and HbSS amplicons. A 565-bp region of the luciferase transgene from transgenic HEK293 cells was also amplified and used as a negative control[76]. Atomic force microscopy (AFM) analysis of the gFET was performed on dCas9 functionalized chips to ensure immobilization of dCas9 onto the surface of the graphene. Figure 2d shows that dCas9 molecules decorate the surface of the graphene channel at a density of 1–2 molecules per μm^2. The immobilized dCas9 was then complexed with either gRNA-HTYa or gRNA-SCDa (Fig. 2e). Both SNP-Chip constructs, termed dCas9-HTYa and dCas9-SCDa, respectively, were calibrated, then the purified amplicon samples ($30\,ng\,\mu l^{-1}$) were introduced to the gFET and incubated on the graphene channel for 25 min at 37 °C. After this incubation period, non-specifically bound DNA was washed away and the final

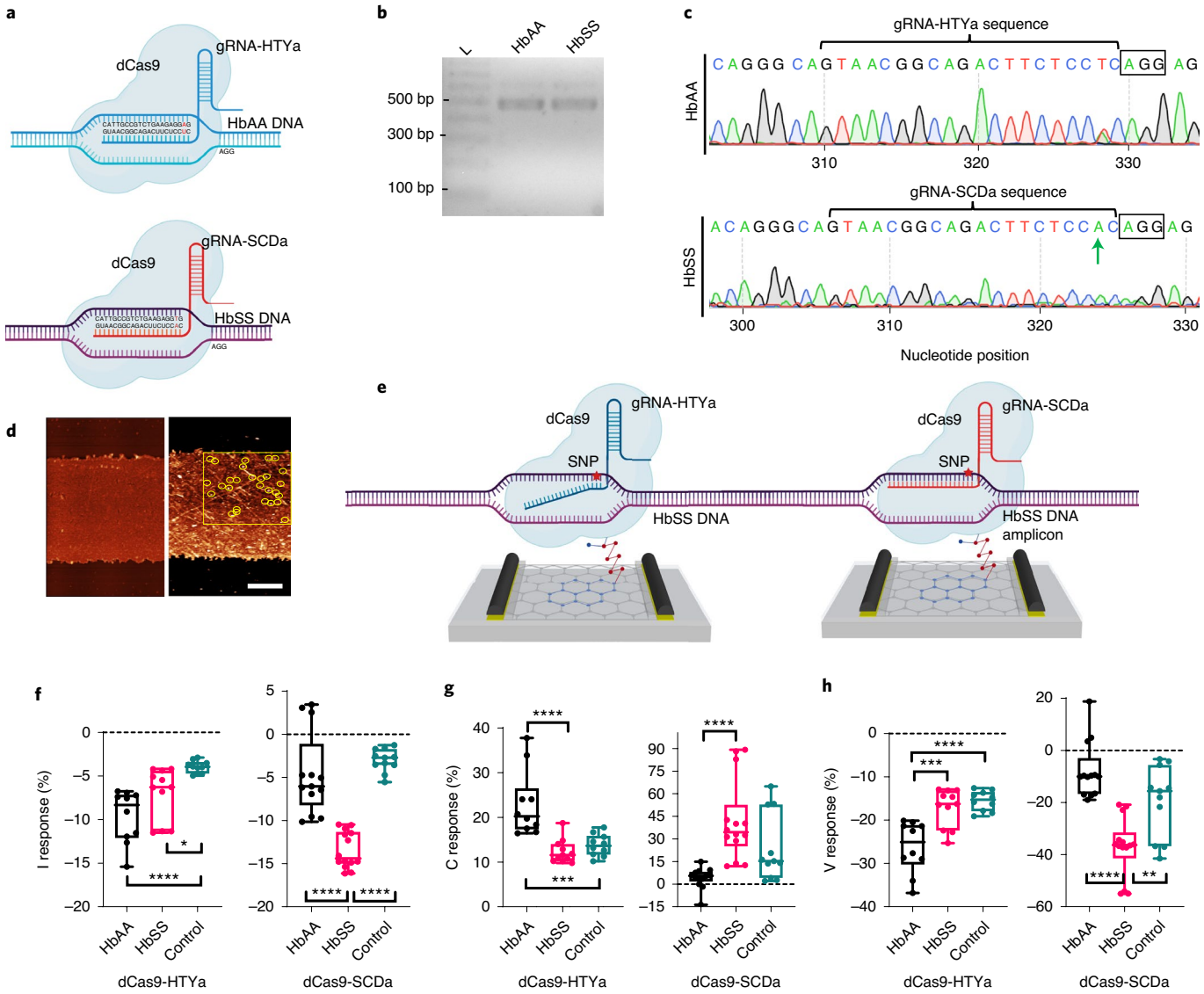

Fig. 2 | SNP-Chip can discriminate between amplicon DNA samples, which differ by a single nucleotide at the gRNA target site. a, gRNA-HTYa was selected to target the HbA allele of the *HBB* gene such that the SCD-associated SNP locus was the second nucleotide upstream of the PAM. The SCD-associated SNP locus is highlighted in red. As a control for the amplicon studies, gRNA-SCDa was designed to target the HbS allele of the *HBB* gene at the same locus as gRNA-HTYa. **b**, 504-bp DNA samples were amplified from HbAA and HbSS genomic DNA templates before CRISPR-based SNP-Chip analysis. L, 100-bp ladder. **c**, Prior to SNP-Chip analysis, HbAA and HbSS DNA amplicons were sequenced to confirm the presence of the target SNP and the gRNA-HTYa and gRNA-SCDa sequences, respectively. The PAM is noted with a black box, and the SCD-associated SNP is noted with a green arrow. **d**, AFM image of a bare graphene channel (left) and a channel after dCas9 immobilization (right). The yellow box indicates a 5 μm × 5 μm graphene area; yellow circles each indicate an immobilized dCas9 molecule. Scale bar, 2 μm. **e**, Schematic of SNP-Chip functionalized with the dCa9–gRNA complex. gRNA-HTYa and gRNA-SCDa were used. In the presence of the SCD-associated SNP, dCas9-HTYa does not hybridize completely with its DNA target, and the DNA dissociates from the dCas9–gRNA complex. For these experiments, all DNA samples were tested at a concentration of 30 ng μl^{-1}. **f**, I response of the dCas9-HTYa construct (left) (one-way analysis of variance (ANOVA): $F = 13.02$) and dCas9-SCDa construct (right) ($F = 41.61$) in the presence of HbAA, HbSS or control amplicons. **g**, C response of the dCas9-HTYa construct (left) ($F = 15.44$) and dCas9-SCDa construct (right) ($F = 11.28$) in the presence of HbAA, HbSS or control amplicons. **h**, V response of the dCas9-HTYa construct (left) ($F = 16.69$) and dCas9-SCDa construct (right) ($F = 20.91$) in the presence of HbAA, HbSS or control amplicons. All box and whisker plots show the minima, Q2, median, Q3 and maxima ($n \geq 10$ technical replicates). Statistical significance was determined by Tukey's multiple comparisons test after one-way ANOVA (*$P < 0.05$; **$P < 0.01$; ***$P < 0.001$; ***$P < 0.0001$; two tailed), $P < 0.05$ considered significant.

DNA signal was analysed relative to the calibration point as a percentage change (Supplementary Fig. 1). The SNP discrimination capability of the dCas9–gRNA SNP-Chip construct is reflected in multiple electrical properties of the gFET channel, reported as the I, C and V responses. The details of the calculations for these values can be found in the Methods and Supplementary Information.

Figure 2f shows the calculated response based on the source–drain current (I response) for both the dCas9-HTYa and dCas9-SCDa constructs after incubation with HbAA amplicons, HbSS amplicons or negative control amplicons. Each data point here represents a freshly functionalized transistor. In the presence of the HbAA amplicon, the dCas9-HTYa SNP-Chip construct had an

average I response value of −9.6%, representing a 2.5-fold increase compared with the negative control and a 1.4-fold increase compared with the SNP-containing HbSS amplicon. A similar separation was observed for the dCas9-SCDa SNP-Chip construct. In the presence of the HbSS amplicon, we saw an average I response value of −13.3% (a 4.4-fold increase relative to the negative control and a 2.9-fold increase relative to the HbAA amplicon). The differences between fully complementary DNA targets (HbAA for gRNA-HTYa and HbSS for gRNA-SCDa) and negative control DNA for both constructs were determined to be significant ($P < 0.0001$; details of the statistical calculations are available in the Methods)[31]. An appreciable difference was observed between DNA samples with and without the SCD-associated SNP. This difference was statistically significant for the dCas9-SCDa SNP-Chip construct ($P < 0.0001$).

Additional discrimination of analytes is possible by evaluating the C and V responses for this dataset. Like the trends observed for the I response, the C response yielded appreciable differences between HbAA and the SNP-containing HbSS amplicons for both SNP-Chip constructs (Fig. 2g). When incubated with its target HbAA amplicon, the dCas9-HTYa construct showed an average response of 22.9% (a 1.9-fold increase in the C response relative to the signal obtained from HbSS amplicons). Similarly, the dCas9-SCDa construct had a C response of 38% (a 9.2-fold increase when incubated with its target HbSS amplicon compared with the HbAA amplicon). Although the variation observed for the C response was larger for the dCas9-SCDa construct, the difference between HbSS and HbAA DNA can still be considered statistically significant ($P < 0.0001$).

The percentage change in the effective gate potential of the graphene relative to calibration (the V response) is shown in Fig. 2h for both SNP-Chip constructs in the presence of HbAA, HbSS or negative control amplicons[66]. Overall, fully complementary amplicons for both dCas9 SNP-Chip constructs produced larger-magnitude V response signals compared with amplicons containing the single-nucleotide mismatch. The average complementary response for dCas9-HTYa was −26.2% and the average complementary response for dCas9-SCDa was −37.0% The control and mismatched samples showed average responses with magnitudes of 24.9% or less. These differences (between complementary and control amplicons and between complementary and mismatch-containing amplicons) were statistically significant ($P \leq 0.03$), consistent with the results observed for I and C responses.

We have consistently observed a difference in the interaction between the dCas9 complex on the surface of the gFET and DNA with varying degrees of complementarity (HbAA, HbSS or control) across all electrical parameters analysed. More specifically, the presence of a single-nucleotide mismatch at the seed region of the protospacer notably decreased the SNP-Chip interaction with amplicons introduced to the sensor. Encouraged by the single-nucleotide specificity of the dCas9-based SNP-Chip, we further examined the sensors' sensitivity in the presence of unamplified genomic DNA targets. For these studies, we employed gRNA-HTYa as this gRNA design demonstrated good specificity in all electrical parameters and has been previously reported to efficiently edit the *HBB* gene at the SCD-associated SNP locus with minimal off-target interactions[75]. Like the SNP-Chip construct used to collect the data presented in Fig. 2f–h, a dCas9-HTYa complex was anchored to the surface of the gFET. This SNP-Chip construct was calibrated and then incubated with unamplified HbAA or HbSS genomic DNA (60 ng μl^{-1}) (Fig. 3a). The I response was measured and the C response was calculated in real time. The C response was selected as the most sensitive measurement parameter in the presence of full genomic DNA. The dCas9-HTYa SNP-Chip construct was able to differentiate between HbAA and HbSS genomic DNA in the C response ($P < 0.0001$). Figure 3c shows representative real-time C response data acquisition for the dCas9-HTYa SNP-Chip in the presence of HbAA and HbSS genomic DNA. This curve shows the change in the C response that occurs with incubation of genomic DNA, followed by the response of the sensor to rinsing off the DNA sample. As a large, charged molecule, DNA creates a large sensing response during incubation regardless of whether the DNA is bound to the CRISPR complex or simply happens to be adjacent to the graphene channel. The real-time data collected indicate that, before removing unbound genomic DNA, a difference between HbAA and HbSS signals can be seen. For example, Fig. 3c shows that within the first 5 min of DNA incubation atop the gFET, HbAA genomic DNA gave a C response signal that was ~1.5-fold larger than that of the HbSS gDNA containing the SNP.

However, the critical measurement occurs at the end of the rinse step, when DNA that is not specifically bound to the CRISPR complex is removed from the surface of the chip. Figure 3d shows the endpoint DNA signal as the C response obtained with the dCas9-HTYa construct after DNA incubation and the final rinse step. The sensor reached equilibrium within 5 min of incubation, suggesting that the assay time can be further reduced (not tested in these studies). These data again show a complementary DNA response greater than 20% (that is, 23.7%), representing a significant 1.6-fold increase in C response ($P < 0.0001$) in the presence of target HbAA genomic DNA compared with the SNP-containing HbSS genomic DNA.

Novel Cas9 variants are continuously being developed for improved specificity[77], thermal stability[78] and size[79]. The growing abundance of Cas9 orthologues has the potential to broaden the applications of SNP-Chip technology. We decided to test this technology with different Cas9 enzymes, including the nuclease-active Cas9 from *Streptococcus pyogenes*, which is the most widely used CRISPR enzyme. Digital analysis of the nuclease-active Cas9 activity can serve as a more direct comparison between SNP-Chip measurements and CRISPR–Cas9 gene therapies targeting pathogenic SNPs, such as those correcting the mutant *HBB* gene via homology-directed repair for SCD gene therapy[57,58]. This was feasible because studies have shown that Cas9 remains bound to DNA post-cleavage[38]. Taking advantage of these findings, we employed an additional SNP-Chip construct, functionalized with a Cas9 (MacroLab, University of California, Berkley)–gRNA-HTYa complex, which is capable of binding to and cleaving the *HBB* target sequence[75].

To interrogate SNP-Chip's capacity to serve as a SNP detection tool when incorporating Cas9 as the CRISPR element, we tested the Cas9-HTYa SNP-Chip construct with both HbAA and HbSS genomic DNA. Figure 3b shows the SNP-Chip construct employed in this study. Figure 3e shows the endpoint DNA signal as the C response obtained with the Cas9-HTYa construct after DNA incubation and the final rinse step. These data show a complementary DNA response of 10.8%, representing a significant 2.4-fold increase in C response ($P = 0.0118$) in the presence of target HbAA genomic DNA compared with the SNP-containing HbSS genomic DNA.

To determine the sensitivity of this platform, we designed the study described in Fig. 3f. The Cas9-HTYa SNP-Chip construct was incubated with varying concentrations of target HbAA genomic DNA (10–60 ng μl^{-1}). The results of this study are shown in Fig. 3g. A positive linear correlation between DNA concentration and C response was observed, indicating the quantitative nature of this technology. To further assess the sensitivity and specificity of the platform, the Cas9-HTYa SNP-Chip construct was incubated in the presence of non-homogenous DNA samples, all of which had a concentration of 60 ng μl^{-1}. These samples contained different percentages of target HbAA DNA and non-target HbSS DNA. The results of this study are shown in Supplementary Fig. 5. A weak positive linear correlation between the percentage of target DNA (HbAA%) and C response was observed, indicating specific discrimination against a concentrated background of DNA with single-nucleotide mismatch specificity. Furthermore, the slope of linear regression

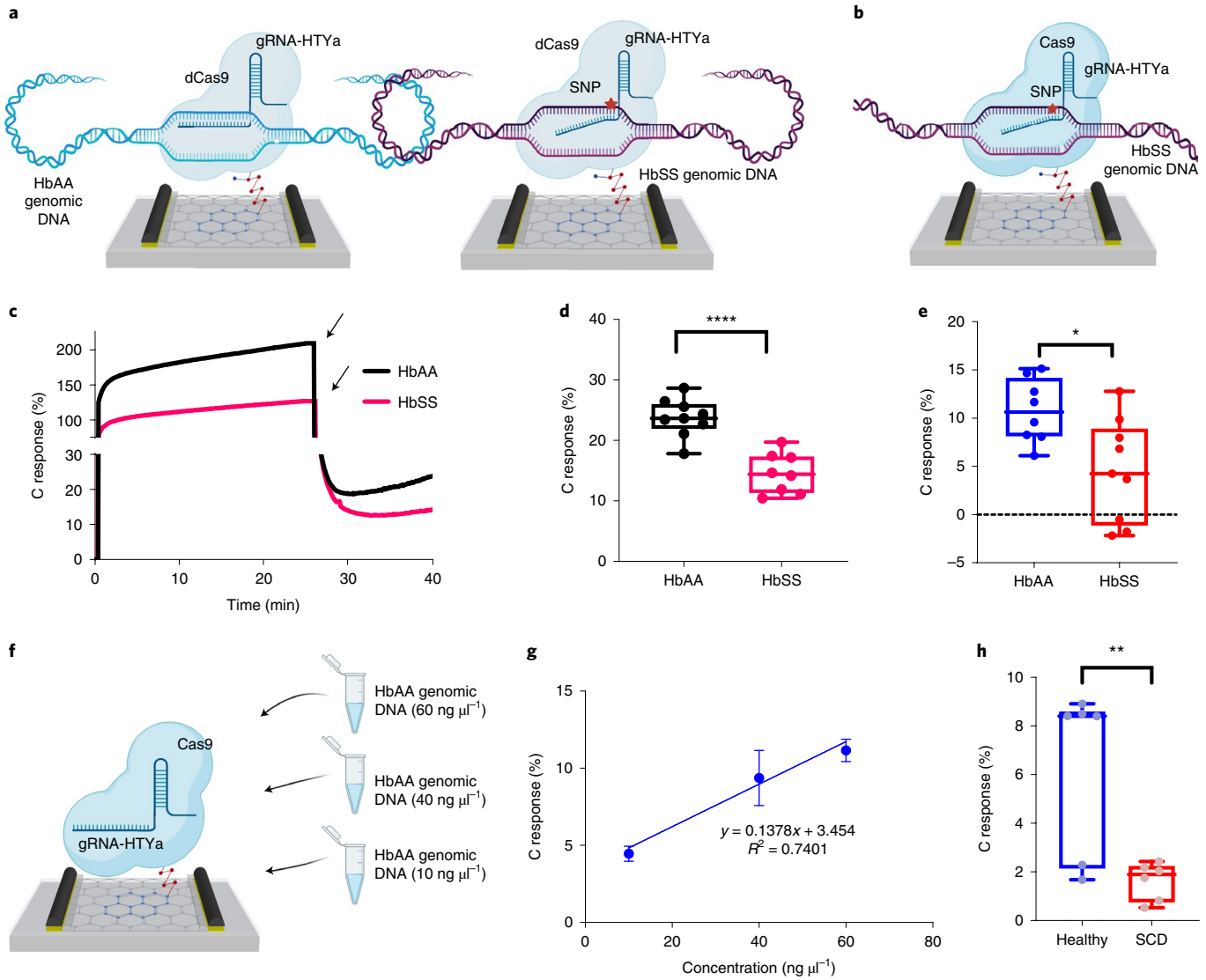

Fig. 3 | dCas9- and Cas9-based SNP-Chip detection of the SCD-associated SNP from genomic DNA samples. a, Schematic of SNP-Chip functionalized with the dCas9–gRNA complex. gRNA-HTYa was used. In the presence of the SCD-associated SNP, dCas9-HTYa does not hybridize completely with its DNA target, and the DNA dissociates from the dCas9–gRNA complex. **b**, Schematic of SNP-Chip functionalized with the nuclease-active Cas9–gRNA complex. gRNA-HTYa was used. **c**, Real-time C response of dCas9-HTYa in the presence of HbAA and HbSS patient genomic samples. The black arrows indicate sensor rinsing. **d**, Endpoint C response of the dCas9-HTYa construct in the presence of HbAA and HbSS patient genomic DNA samples (60 ng μl^{-1}) ($t = 5.849$; d.f. = 15; $n \geq 8$ technical replicates). **e**, Endpoint C response of SNP-Chip with the nuclease-active Cas9-HTYa construct after incubation with homozygous HbAA and HbSS patient genomic DNA samples (60 ng μl^{-1}) ($t = 2.867$; d.f. = 15; $n = 8$ technical replicates). **f**, Schematic of the sensitivity test during which the nuclease-active Cas9-HTYa construct was incubated with varying concentrations of target HbAA DNA samples (10–60 ng μl^{-1}). **g**, Results of the Cas9-HTYa construct sensitivity test, during which the nuclease-active Cas9-HTYa construct was incubated with varying concentrations of target HbAA DNA samples (10–60 ng μl^{-1}). Each point in the scatter plot shows a mean value ± s.d. ($n \geq 5$ technical replicates). **h**, Results of blind studies of the C response of SNP-Chip functionalized with nuclease-active Cas9-HTYa in the presence of patient samples with each phenotype (healthy or SCD) ($t = 3.325$; d.f. = 10; $n = 3$ biological replicates, with two technical replicates per biological sample). In **d**, **e** and **h**, significance was determined by unpaired *t*-test (*$P < 0.05$; **$P < 0.01$; ****$P < 0.0001$; all two tailed). All box and whisker plots show the minima, Q2, median, Q3 and maxima.

deviated significantly from zero ($P = 0.0072$). The lowest concentration of target HbAA DNA tested in this study was 12 ng μl^{-1}, which, when considering a molecular weight of 1.9×10^{12} g mol^{-1} of the human genome[80], equals 6.3 fM. To confirm SNP-Chip's ability to discriminate between target and non-target DNA at this concentration, an additional experiment was performed in which the Cas9-HTYa construct was incubated with 6.3 fM HbAA genomic DNA and 6.3 fM HbSS genomic DNA (Supplementary Fig. 3). At a concentration of 6.3 fM, SNP-Chip was still capable of discriminating between HbAA and HbSS DNA ($P = 0.03$).

We obtained multiple genomic samples isolated from three patients with SCD and three healthy individuals (Coriell Institute). Specifications of these samples are described in Supplementary Table 3. In addition to the two SCD samples, which are homozygous for the E6V mutation, we also tested a sample that had the E6V mutation on one allele and the single-nucleotide variant at codon 6 of the *HBB* gene (that is, a glutamic acid to lysine amino acid substitution of the *HBB* gene; E6K) on the other allele. This mutation results in the production of mutant haemoglobin C, as well as mutant haemoglobin S (HbS). This sample has the genotype E6V/E6K.

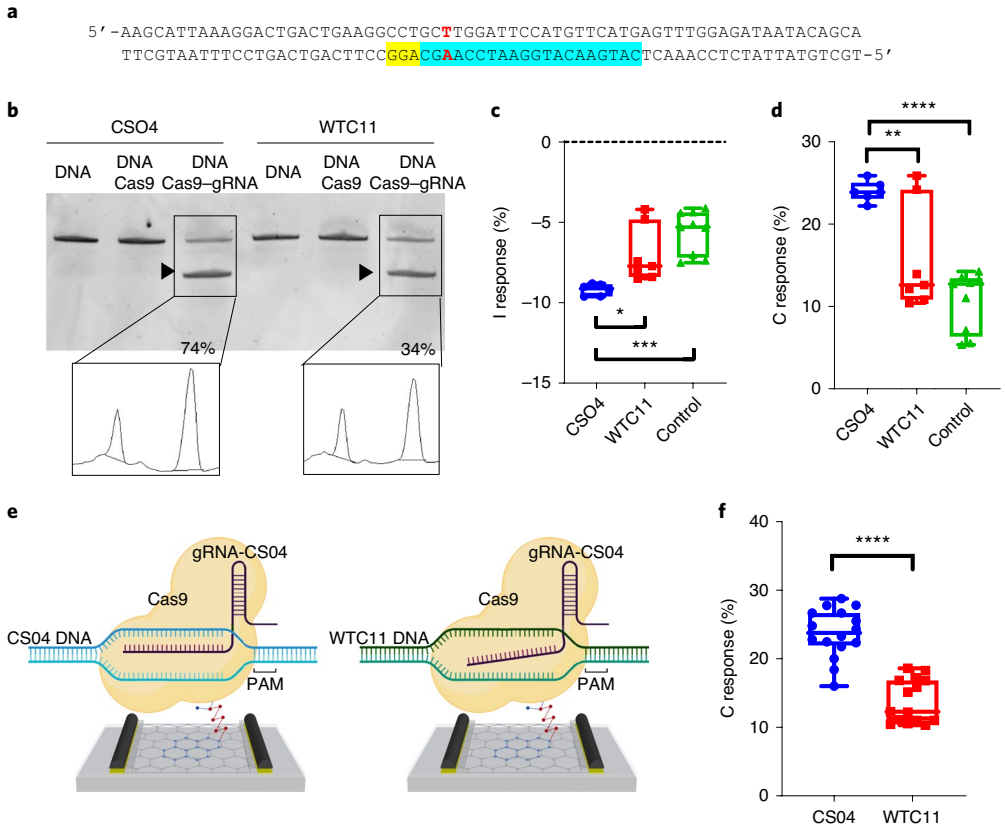

Fig. 4 | SNP-Chip can differentiate between samples with and without a *SOD1* SNP. a, gRNA-CS04 was designed to target the fALS-associated H44R SNP (red) three nucleotides from the PAM (yellow). The gRNA target is highlighted (blue). **b**, In vitro cleavage assay with gRNA-CS04 and CS04 and WTC11 amplicons shows more efficient cleavage of CS04 than WTC11. The cleavage products are indicated by black arrowheads. The percentage cleavage was determined with ImageJ. **c**, I response of the Cas9-CS04 construct in the presence of CS04, WTC11 and negative control amplicons ($n \geq 5$ technical replicates; $F = 13.02$). **d**, C response of the Cas9-CS04 construct in the presence of CS04, WTC11 and negative control amplicons ($n \geq 5$ technical replicates; $F = 16.7$). Significance in **c** and **d** was determined by Tukey's multiple comparisons test after one-way ANOVA (*$P < 0.05$; **$P < 0.01$; ***$P < 0.001$; ****$P < 0.0001$), with $P < 0.05$ considered significant. **e**, Schematic of the Cas9-CS04 construct in the presence of CS04 and WTC11 genomic DNA. **f**, C response in the presence of CS04 and WTC11 genomic DNA (60 ng μl^{-1}) ($t = 8.131$; d.f. = 29; $n \geq 16$ technical replicates). Significance was determined by two-tailed unpaired *t*-test (****$P < 0.0001$). All box and whisker plots show the minima, Q2, median, Q3 and maxima.

Blind testing of these samples with the Cas9-HTYa SNP-Chip construct was performed. Again, SNP-Chip could discriminate between samples from healthy individuals and patient samples that contained a SNP within the Cas9 target site ($P = 0.0077$) (Fig. 3h).

To demonstrate the broader usability of SNP-Chip, we employed a second human disease model based on a single-nucleotide mutation in the human *SOD1* gene. This mutation had an A to T substitution resulting in an amino acid substitution of histidine for arginine at codon 44 (H44R) in the SOD1 protein. Specific mutations in the *SOD1* gene, such as H44R, have been linked to the onset of fALS[81]. We designed a gRNA to target the H44R mutation within SOD1. This gRNA, termed gRNA-CS04, was compatible with Cas9 and targeted the H44R SNP at the third nucleotide from the PAM (Fig. 4a). To validate the SNP specificity of gRNA-CS04, we performed an in vitro cleavage assay with target amplicons (CS04 amplicons) originating from hiPSCs, which carried the H44R mutation. As a control, wild-type hiPSCs were also obtained, and the H44R locus was also amplified. These amplicons containing the wild-type sequence are referred to as WTC11. After 30 min, when complexed with Cas9, gRNA-CS04 showed more efficient cleavage activity with its target amplicon (CS04), as quantified by ImageJ software. Cleavage activity of the target amplicon was 74%, compared with the activity observed with the wild-type amplicon (WTC11), which was 34% (Fig. 4b). We then tested the Cas9-CS04 SNP-Chip construct with CS04, WTC11 and negative control amplicons at a concentration of 30 ng μl^{-1}. In both the I response and the C response, SNP-Chip could discriminate between amplicons, which differed by a single nucleotide ($P \leq 0.0216$) (Fig. 4c,d).

Finally, to further confirm the ability of SNP-Chip to discriminate between samples that differ by a single nucleotide in the fALS disease model (in addition to the SCD model) without amplification, we extracted genomic DNA from wild-type hiPSCs (termed WTC11) and hiPSCs, which carried the H44R mutation in the *SOD1* gene (termed CS04). Genomic DNA samples (60 ng μl^{-1}) were introduced to the Cas9-CS04 SNP-Chip construct (Fig. 4e). In the presence of its target DNA, the Cas9-CS04 SNP-Chip construct had an average C response of 23.7%, which was significantly larger than the C response obtained from the same construct in the presence of the WTC11 genomic DNA sample ($P < 0.0001$). One device was determined to be an outlier by Grubb's outlier test and was removed from further analysis. These results demonstrate that SNP-Chip can be reconfigured to target different SNPs of interest by simply redesigning the gRNA component of the SNP-Chip construct.

Although Cas9 is highly programmable[74], single-base-pair sensitivity is limited by the location of that base pair relative to the PAM. The primary PAM for Cas9, 5′-NGG-3′, occurs every 8–12 bp in the human genome on average[82,83]; however, it is possible that for an arbitrary SNP, gRNA designs for Cas9 would not be sufficient for

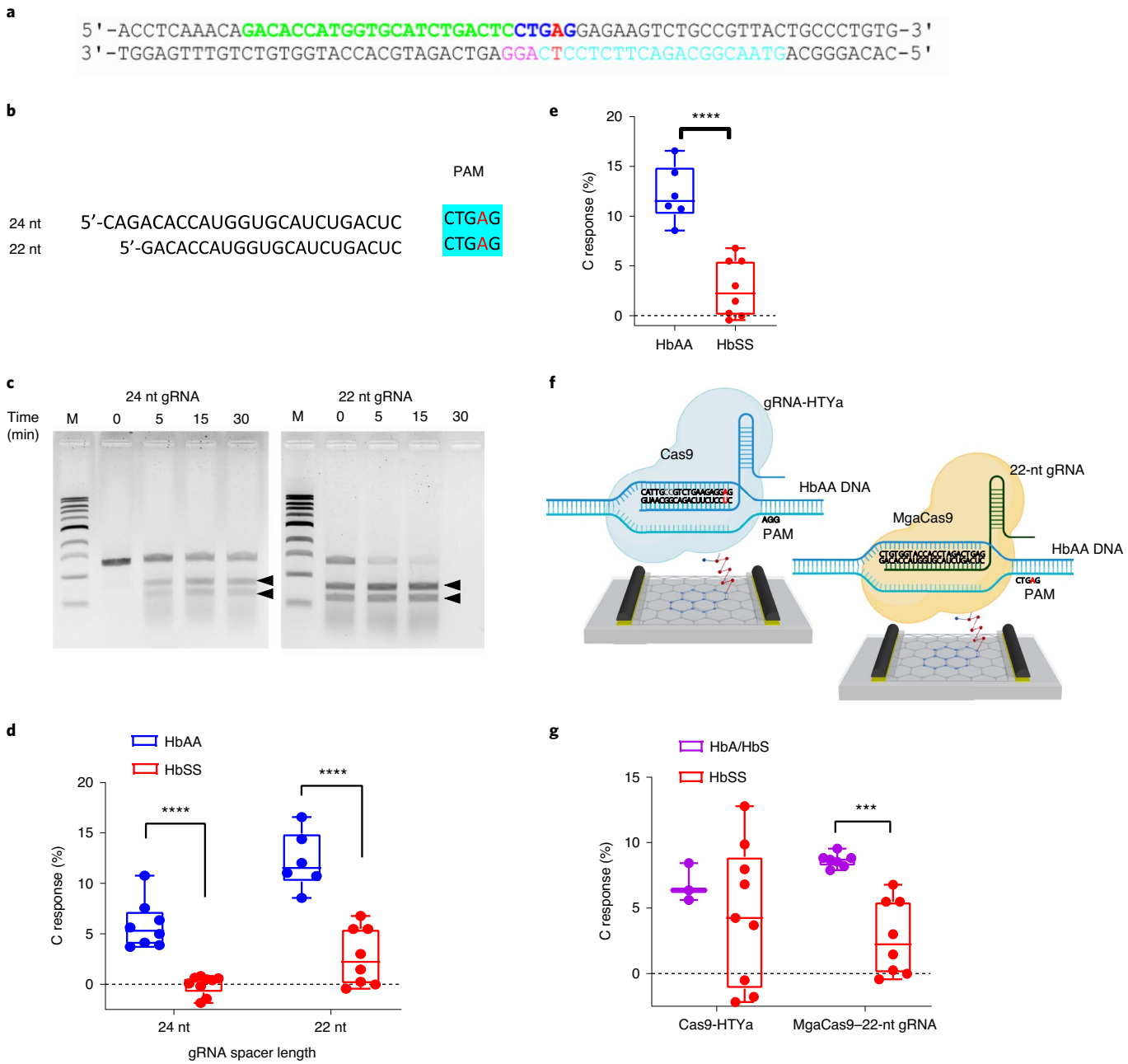

Fig. 5 | The MgaCas9 SNP-Chip construct can assess gRNA activity and heterozygosity. a, Schematic of MgaCas9 and Cas9 targets in the *HBB* gene. The SNP is indicated in red, the MgaCas9 target sequence is indicated in green and its PAM is indicated in blue. The Cas9 PAM and protospacer are on the opposite DNA strand and are indicated in pink (PAM) and blue (target sequence). **b**, Two different MgCas9-compatible gRNAs were designed to target the SCD-associated SNP locus (red) in the PAM (highlighted in blue) with two spacers of different nucleotide (nt) lengths. **c**, An in vitro cleavage assay was performed on *HBB* amplicons, and successful cleavage was confirmed via gel electrophoresis. The 22-nucleotide gRNA was more efficient than the 24-nucleotide gRNA after a 30-min reaction, as indicated by the double arrowheads. M, 1-kb DNA ladder. **d**, Two SNP-Chip constructs utilizing MgaCas9 were employed to compare the efficiencies of the 22-nucleotide gRNA and the 24-nucleotide gRNA. The C response of the MgaCas9–22-nucleotide gRNA construct ($t = 6.143$; d.f. = 12) and the MgaCas9–24-nucleotide gRNA construct ($t = 6.897$; d.f. = 15) in the presence of homozygous HbAA and HbSS patient genomic DNA samples (60 ng μl^{-1}) was measured ($n \geq 6$ technical replicates). **e**, C response of the SNP-Chip MgaCas9–22-nucleotide gRNA construct after incubation with homozygous HbAA and HbSS patient genomic DNA samples (60 ng μl^{-1}) ($n \geq 6$ technical replicates). **f**, Schematic of the SNP-Chip Cas9-HTYa construct fully complexed with the target HbAA genomic DNA (left) and the SNP-Chip MgaCas9–22-nucleotide gRNA construct fully complexed with the target HbAA genomic DNA (right). **g**, C response of the SNP-Chip Cas9-HTYa construct ($t = 0.7082$; d.f. = 10) and the MgaCas9–22-nucleotide gRNA construct ($t = 5.362$; d.f. = 13) after incubation with heterozygous HbA/HbS and homozygous HbSS patient genomic DNA samples (60 ng μl^{-1}) ($n \geq 3$ technical replicates). Significance in **d**, **e** and **g** was determined by two-tailed unpaired *t*-test (***$P < 0.001$; ****$P < 0.0001$). All box and whisker plots show the minima, Q2, median, Q3 and maxima.

SNP detection. This limitation could be addressed by incorporating CRISPR enzymes that interact with different PAMs[84–86] into the SNP-Chip design or by employing high-fidelity CRISPR enzymes that have enhanced SNP sensitivity[41,42]. We hypothesized that a Cas9 orthologue that targets the SCD-associated SNP within the PAM would further improve SNP-Chip's sensitivity. Namely, since

a single-nucleotide mutation in the PAM abolishes binding and cleavage by Cas9 (refs. [74,87]), SNPs located within the PAM sequence should compromise Cas9 binding and improve SNP-Chip's SNP discrimination capability. We have recently identified a Cas9 orthologue from *Mycoplasma gallisepticum* CA06 strain (MgaCas9; CasZyme) that recognizes 5′-NNGAD-3′ PAM (where D is any nucleotide except C)[88], which overlaps with the SCD-associated SNP (Fig. 5a). This Cas9 orthologue is characterized by a short gRNA, with only two hairpin structures. Also, the analysis of melting temperatures indicated that the thermostability of MgaCas9 is comparable to that of Cas9 (ref. [88]).

To establish gRNA requirements for MgaCas9, we determined the optimal spacer length with an in vitro DNA cleavage assay. We PCR amplified the *HBB* gene fragment and monitored MgaCas9 cleavage using 21-, 22-, 23- and 24-nucleotide protospacer gRNAs that targeted *HBB* at the same location such that the SCD-associated SNP locus was in the PAM (Fig. 5a,b and Supplementary Fig. 2). The most efficient cleavage occurred after 30 min with the 22-nucleotide spacer gRNA (Fig. 5c and Supplementary Fig. 2).

We then tested whether SNP-Chip could serve as a facile amplification-free tool for designing and selecting Cas complexes with higher efficiency, thereby improving on conventional methods for the selection of different RNA-guided Cas enzymes. To do this, two iterations of SNP-Chip, functionalized with MgaCas9, were employed using two of the validated MgaCas9 gRNA designs. When the two MgaCas9 constructs were incubated with DNA samples, both constructs were able to discriminate between HbAA and HbSS genomic DNA with statistical significance ($P < 0.0001$) (Fig. 5d). These results obtained from the SNP-Chip MgaCas9 constructs also indicated higher efficiency of the 22-nucleotide gRNA (Fig. 5d,e), in agreement with the results from the in vitro cleavage assay. This result suggests that this technology can monitor gRNA designs without the need for amplification, which could simplify the gRNA validation process.

In addition, the MgaCas9–22-nucleotide gRNA construct was tested in the presence of non-homogeneous genomic DNA samples that contained different proportions of target (HbAA) and non-target (HbSS) genomic material. Notably, using the MgaCas9–22-nucleotide gRNA compared with the Cas9-HTYa construct improved the linear correlation (R^2) between HbAA% and the C response (Supplementary Fig. 5). The slope of this linear regression also deviated significantly from zero ($P < 0.0001$), suggesting that altering the CRISPR component of SNP-Chip can improve its quantitative capabilities.

Finally, we assessed the ability of SNP-Chip to measure the heterozygosity of SNPs without DNA amplification. For this study, we obtained genomic material from a patient heterozygous for HbA and HbS alleles (Coriell Institute). This heterozygous sample (HbA/HbS) was analysed using both the Cas9-HTYa SNP-Chip construct and the MgaCas9–22-nucleotide gRNA construct. A schematic of the gRNA target sequences and PAM of these two constructs is shown in Fig. 5f. We have shown that the Cas9-HTYa SNP-Chip construct can discriminate between HbAA and HbSS DNA, but it was unable to discriminate between heterozygous (HbA/HbS) and homozygous (HbSS) samples (Fig. 5g). However, the MgaCas9–22-nucleotide gRNA construct, which targeted the SCD-associated SNP within the PAM, discriminated directly (no DNA amplification) between the homozygous (HbSS) and heterozygous (HbA/HbS) samples with statistical significance ($P = 0.000129$). This result is important in demonstrating the ability of SNP-Chip to detect heterozygosity, to quantify predisposition to and potential to transmit numerous genetic disorders by taking advantage of the diversity of Cas9 orthologues and the programmability of SNP-Chip.

Discussion

The use of gFET sensors has become a powerful and useful tool for detecting biomolecules in medical, clinical, agricultural and environmental applications as they offer great versatility and high sensitivity[67,89–92]. In our previous study, we combined CRISPR–dCas9 with our graphene transistors to harness the power of CRISPR as a nucleic acid search and targeting engine[31]. In this study, we have further expanded the uses of this technology by incorporating different CRISPR–Cas9 variants and expanding the types of electrical measurements taken to yield a rapid and direct electronic CRISPR-based biosensor for SNP detection (SNP-Chip) without the need for DNA amplification.

Although other SNP detection technologies have been reported[64,93–95], these technologies primarily interact with small DNA fragments[65,94] or the less complex bacterial genome[93]. SNP detection in the more complex human genome requires enrichment[96] or amplification[64]. More detailed comparisons between our technology and other DNA detection technologies are available in Supplementary Tables 1 and 2.

To evaluate the technology, we first tested SNP-Chip using SCD as a SNP disease model. By using a gRNA to target the healthy *HBB* allele, such that the SNP locus was within the seed region of the gRNA spacer sequence, SNP-Chip constructs with both dCas9 and Cas9 could discriminate between genomic DNA samples from healthy patients and those with SCD. We have also tested this technology in the presence of non-homogenous DNA samples containing different percentages of target versus non-target DNA, demonstrating the quantitative nature of this technology. One key advantage of using CRISPR–Cas9 and SNP-Chip label-free technology is the ease of re-programmability to detect other target genes. To target a different mutation, one can reconfigure the CRISPR element employed within SNP-Chip by simply designing a new gRNA. We have demonstrated this by utilizing SNP-Chip to detect a different single-nucleotide mutation implicated in human disease (ALS). These findings suggest that facile SNP-sensitive genotyping of multiple genes is possible with CRISPR-powered gFETs.

One key limitation of this technology is the PAM-dependent nature of CRISPR–Cas9 to interact and bind to its DNA target[33], as this interaction is reliably disrupted when mismatches lie in the PAM-proximal region of the gRNA spacer sequence[71]. Therefore, certain single-nucleotide mutations, which are not proximal to a PAM sequence, may be difficult to detect. Although this presents a challenge for broad applications of this technology, the diversity of newly discovered Cas9 orthologues or engineered Cas9 variants, including those that are PAM independent[97], will enable further expansion of our technology's capability to detect a wide variety of gene sequences with SNP-level sensitivity. For example, in this work, we have used a recently reported Cas9 orthologue[88] with different PAM requirements to improve the discriminative capability of our platform. The use of this Cas9 orthologue enabled us to discriminate between genomic DNA from patients homozygous for the sickle cell trait and patients who were heterozygous carriers of the trait. The CRISPR field is constantly expanding, and as new CRISPR–Cas enzymes are discovered or engineered, the potential applications of this technology will broaden, allowing us to develop new tools for rapid and facile nucleic acid detection.

SNP-Chip may contribute to medical diagnostics and basic research, as it can meaningfully reduce the time and cost of SNP genotyping, monitor the efficiency of gRNA designs and facilitate the quality control processes involved in CRISPR-based gene editing.

Methods

AFM. AFM images of the graphene FET chip surfaces were acquired in 20 μm × 20 μm areas with 512 pixel × 512 pixel resolution and a scan rate of 0.5 Hz in non-contact, tapping mode using the Pacific Nanotechnology Nano-R_2 scanning probe microscope. Images were analysed using Gwyddion.

dCas9, Cas9 and MgaCas9 gRNA design. Multiple gRNAs were designed for SCD detection on SNP-Chip. gRNA-HTYa targets the sequence

5′-GTAACGGCAGACTTCTCCTC-3′ and is specific to the wild-type HbA *HBB* allele, which does not contain the single-point mutation associated with SCD. Briefly, it has previously been reported that gRNA-HTYa facilitates the cleavage of the *HBB* target sequence[75]. gRNA-SCDa targets the sequence 5′-GTAACGGCAGACTTCTCCAC-3′ and is specific to the HbS sickle cell trait, which contains the single-point mutation associated with SCD. For both gRNA-HTYa and gRNA-SCDa, the SCD-associated SNP locus occurs in the second nucleotide of the protospacer sequence proximal to the PAM. Both gRNA-HTYa and gRNA-SCDa are compatible with dCas9 and Cas9 (ref. [36]). The third gRNA, which is compatible with MgaCas9 (CasZyme), targets the wild-type HbA allele. This MgaCas9 gRNA targets the sequence 5′-GACACCATGGTGCATCTGACTC-3′. The MgaCas9 gRNAs used in this study were synthesized by in vitro transcription using HiScribe T7 Quick High Yield RNA Synthesis kits (New England Biolabs (NEB)) and purified using the Monarch RNA Cleanup Kit (NEB). RNA concentration and purity were measured using a NanoPhotometer NP80 (Implen), and RNA integrity was visualized by 2% agarose electrophoresis. One gRNA was designed for the ALS model. This gRNA targets the sequence 5′-CATGAACATGGAATCCAAGC-3′ and was ordered from Synthego without modification.

DNA cleavage assay. MgaCas9 (CasZyme) was purified and 50 µl MgaCas9–gRNA complex was assembled by incubating 0.08 µM MgaCas9 and 0.16 µM Cas9 gRNA in assembly buffer (10 mM Tris-HCl, 100 mM NaCl, 1 mM ethylenediaminetetraacetic acid (EDTA) and 1 mM dithiothreitol (pH 7.5)) at 20 °C for 1 h. Then, 50 µl 5 nM target DNA in 1× CutSmart Buffer (NEB) was also prepared and heated to 37 °C. A 20 µl 1:1 vol/vol mix of preheated target DNA mix and MgaCas9–gRNA complex was incubated for 30 min at 37 °C. Afterwards, 5.6 µl 6× Gel Loading Dye, Blue (NEB) was added to the reaction. Cleavage was visualized via 1% agarose gel electrophoresis. The complex is considered active if 40 nM of the complex cleaves 100% of 2.5 nM DNA within 30 min at 37 °C and if 20 nM of the complex cleaves at least 80% of 2.5 nM DNA within 30 min at 37 °C.

Purified Cas9 (MacroLab) was complexed with gRNA-CS04 by mixing 50 µl 80 nM Cas9 and 80 nM gRNA in Assembly Buffer (10 mM Tris-HCl, 100 mM NaCl, 1 mM EDTA and 1 mM dithiothreitol (pH 7.5)) at 20 °C for 1 h. Then, 50 µl 10 nM target DNA in 1× CutSmart Buffer (NEB) was also prepared. A 20 µl 1:1 vol/vol mix of preheated target DNA mix and Cas9–gRNA complex was incubated for 30 min at 37 °C. Afterwards, 5.6 µl 6× Gel Loading Dye, Blue (NEB) was added to the reaction. The reaction was then incubated at 85 °C for 10 min. The reaction was run on a 10% polyacrylamide gel (Bio-Rad) for 45 min at 110 V and stained with SYBR Gold. The band intensity was quantified with ImageJ.

Clinical DNA samples. Human genomic samples were obtained with a certificate of analysis from the Coriell Institute for Medical Research. The HbAA sample (NA03798) was from a 10-year-old healthy Caucasian male. The HbSS sample (NA16265) was from a 19-year-old African American male homozygous for SCD. The HbA/HbS sample (NA20838) was from a 35-year-old African American female heterozygous for the SCD trait. The concentrations were routinely measured before use via Nanodrop One (Thermo Scientific).

Culture of hiPSCs and mutation screening. hiPSCs (WTC11) were obtained through the University of California, Berkeley Cell Culture Facility. The *SOD1*-mutated fALS iPSCs (CS04) were obtained from the Cedars-Sinai Medical Center (Los Angeles, California). All hiPSCs were maintained on plates coated with Vitronectin (Life Technologies) and cultured in Essential 8 Medium (Life Technologies) at 37 °C under a 5% CO_2 atmosphere. All hiPSCs were passaged every 7 d by 0.5 mM EDTA (Life Technologies). Genomic DNA was extracted using DNeasy Blood & Tissue kits (Qiagen) according to the manufacturer's instructions. For PCR amplification of the H44R region in *SOD1* (NM_000454.5), the following primers were used: 5′-GGGTGCTTGTGCATTGAGTG-3′ (forward) and 5′-GGGTTTTAACGTTTAGGGGCT-3′ (reverse). The PCR protocol can be found in the 'PCR amplification' section below. The products were directly sequenced using the 3130 Genetic Analyzer (Applied Biosystems).

PCR amplification. The following PCR protocol was used to amplify a 504-bp region of the *HBB* gene from both HbAA and HbSS gDNA templates: 50 ng genomic DNA (NA03798 or NA16265), 1× Phusion HF Buffer, 200 µM dNTP, 0.5 µM forward primer, 0.5 µM reverse primer and 1 U Phusion DNA polymerase (NEB). The final volume of the PCR reaction was 50 µl. The forward and reverse primer sequences were 5′-TTGAGGTTGTCCAGGTGAGCCA-3′ and 5′-GGCCAATCTACTCCCAGGAGCA-3′, respectively. The following thermal cycler protocol was used: (1) 98 °C for 30 s; (2) 98 °C for 10 s; (3) 63.5 °C for 30 s; (4) 72 °C for 15 s; (5) repeat steps 2–4 29 times; and (6) hold at 72 °C for 5 min before cooling to 4 °C. HbAA and HbSS sequences were validated via Sanger sequencing using the same primers mentioned previously. Sanger sequencing was performed by the University of California, Riverside Gene Core.

A luciferase-transgenic HEK293 cell line (Luc14 HEK293)[76] was used to amplify a 565-bp negative control sequence via a nested PCR protocol. This amplicon did not contain the gRNA-HTYa or the gRNA-SCDa target sequences. The forward and reverse primer sequences for the first PCR were 5′-GCTCACTCATTAGGCACCCC-3′ and 5′-GGCGTTGGTCGCTTCCGGAT-3′, respectively. For the second (nested) PCR, the forward and reverse primer sequences were 5′-CACTTTATGCTTCCGGCTCG-3′ and 5′-CCGCGTACGTGA TGTTCACC-3′, respectively. All amplicons were confirmed on a 1% agarose gel, stained with 0.5 µg ml^{-1} ethidium bromide for 30 min and imaged using UVP ChemStudio (Analytik Jena). All final PCR-derived amplicons were purified using a PureLink PCR Purification Kit (Invitrogen) before SNP-Chip experiments.

A 2,058-bp DNA fragment for the MgaCas9 cleavage assay was obtained by PCR using as a template HEK293 (ATCC; CRL-1573) genomic DNA and a 5′-TCCTGAGACTTCCACACTGATGC-3′ and 5′-TGCACAGAGCACATT GATTTGT-3′ primer pair. The PCR product was purified using Monarch DNA Cleanup and Gel Extraction (NEB). The MgaCas9–gRNA complex cleaves a 1,305-bp DNA substrate to generate 736- and 569-bp products.

A 417-bp region of the *SOD1* gene encompassing the H44R SNP locus was amplified from 50 ng template CS04 and WTC11 genomic DNA using the Phusion High-Fidelity PCR Kit (NEB). Reactions were prepared according to the manufacturer's protocol. The forward and reverse primer sequences were 5′-GGGTGCTTGTGCATTGAGTG-3′ and 5′-GGGTTTTAACGTTTAGGGGCT-3′, respectively. The following PCR protocol was used: (1) 98 °C for 3 min; (2) 98 °C for 10 s; (3) 62 °C for 30 s; (4) 72 °C for 15 s; (5) repeat steps 2–4 34 times; (6) 72 °C for 10 min; and (7) hold at 4 °C.

SNP-Chip gFET functionalization via molecular linker absorption, activation, Cas enzyme coupling, passivation and Cas–gRNA complex formation. For the amplicon studies, gFETs (Cardea) were rinsed with 30 µl acetone twice, followed by two rinses with 30 µl deionized water. The chips were subsequently functionalized with PBA (5 mM; 15 µl; Sigma–Aldrich) in dimethylformamide (DMF) for 2 h at room temperature. Following the incubation, the gFETs were rinsed twice with 30 µl DMF, followed by 30 µl deionized water. The functionalized PBA gFETs were then air dried and used immediately or stored at 4 °C for later use. PBA was activated using a 1:1 vol/vol ratio of *N*-(3-dimethylaminopropyl)-*N*′-ethyl carbodiimide hydrochloride (EDC, 4 mM) and *N*-hydroxysuccinimide (NHS; 11 mM; Sigma–Aldrich) in 50 mM 2-(*N*-morpholino)ethanesulfonic acid (MES; pH 6) for 5 min at room temperature before incubation with Cas enzyme[98,99]. Cas enzymes (900 ng in 30 µl 2 mM $MgCl_2$) were incubated atop the gFET for 15 min, after which the gFET was rinsed twice with 30 µl MES (pH 6). Any uncoupled PBA molecules on the graphene surface were then blocked using amino-PEG_5-alcohol (1 mM; 10 min) and ethanolamine hydrochloride (1 M; 10 min). The surface was then rinsed five times with 2 mM $MgCl_2$ to remove any unbound blocking agent for 1 min. The chips were then calibrated for gRNA using 2 mM $MgCl_2$ for 5 min. gRNA (900 ng in 30 µl 2 mM $MgCl_2$) was then incubated on the gFET for 10 min at 37 °C. The surface was then rinsed with 2 mM $MgCl_2$ to remove any unbound gRNA for 5 min. The distribution of the biofunctionalization signals can be found in Supplementary Fig. 4.

For the genomic studies, gFETs (Cardea) were rinsed with 30 µl acetone followed by 30 µl deionized water twice. The gFETs were subsequently functionalized with PBA (750 mM; 15 µl; Sigma–Aldrich) in DMF for 1 h at room temperature. Following the incubation, the gFET chips were rinsed with 30 µl DMF followed by 30 µl 70% ethanol twice and 30 µl 100% isopropyl alcohol. The functionalized PBA chips were then air dried and used immediately or stored at 4 °C for later use. PBA was activated using a 1:1 vol/vol ratio of EDC (200 mM) and NHS (400 mM) (Sigma–Aldrich) in 50 mM MES (pH 6) for 5 min at room temperature before incubation with Cas enzymes. Cas enzymes (900 ng in 2 mM $MgCl_2$) were incubated atop the gFET for 15 min, after which the gFET was rinsed twice with 30 µl MES (pH 6). Any uncoupled PBA molecules on the graphene surface were then blocked using amino-PEG_5-alcohol (1 mM; 10 min) and ethanolamine hydrochloride (1 M; 10 min). The surface was then rinsed five times with 2 mM $MgCl_2$ to remove any unbound blocking agent for 1 min. The chips were then calibrated for gRNA using 2 mM $MgCl_2$ for 5 min. gRNA (900 ng in 2 mM $MgCl_2$) was then incubated on the chip for 10 min at 37 °C. The surface was then rinsed with 2 mM $MgCl_2$ to remove any unbound gRNA for 5 min.

SNP-Chip calibration and DNA detection on functionalized gFETs. To compare sensor responses from different devices, each chip was incubated in a solution of 2 mM $MgCl_2$ for 5 min immediately before the introduction of DNA to allow for equilibration of the graphene surface, which we refer to as sensor calibration. All signals following calibration were calculated and expressed as a percentage change from the final signal during calibration. DNA samples were then incubated atop the gFET for 25 min (30 ng µl^{-1} in 2 mM $MgCl_2$ for the amplicon studies and 60 ng per 30 µl in 2 mM $MgCl_2$ for the genomic DNA studies). Any unbound DNA was then rinsed with 2 mM $MgCl_2$ for 15 min. Cas9 and MgaCas9 genomic DNA was rinsed for an additional 5 min. All steps in the assay were performed at 37 °C. The temperature was controlled with a benchtop incubator.

Sensitivity and specificity studies. Sensitivity studies were performed by incubating varying concentrations (10–60 ng µl^{-1}) of HbAA genomic DNA (NA03798). These were then tested on the SNP-Chip Cas9-HTYa construct according to the protocol defined in the section 'SNP-Chip calibration and DNA detection on functionalized gFETs'. Specificity studies were performed by creating

non-homogeneous mixtures of HbAA (NA03798) and HbSS (NA16267) genomic DNA, all of which had a final concentration of 60 ng μl^{-1}. These were then tested on SNP-Chip Cas9-HTYa and MgaCas9–22-nucleotude gRNA constructs according to the protocol defined in the section 'SNP-Chip calibration and DNA detection on functionalized gFETs'.

Blind studies. SNP-Chip blind studies were performed by first obtaining three genomic DNA samples each from healthy patients (NA03798, NA22807 and NA23904) and patients with SCD (NA16265, NA16266 and NA16267) from the Coriell Institute for Medical Research. Samples were tested and analysed blind. For all other electrical measurements presented in this manuscript, technical replicates were employed. This was due to the nature of this work and the importance of sensor reproducibility. In the blinded studies, we employed biological replicates by assaying samples with either healthy or diseased phenotypes (Fig. 3h).

SNP-Chip sensor response, measurement and analysis methods. The Agile R100 reader system (Cardea) was used for all measurements using the standard electrical setting. Each chip consisted of three transistors (gFETs) using a shared counter and reference electrodes. Each transistor consisted of five graphene channels in parallel. The gate voltage was swept from −100 to +100 mV continuously, at a constant rate, while the source–drain current through each transistor was monitored and recorded in real time. I, C and V response values were calculated for each cycle of a triangular gate loop and were always referenced to a calibration step before the addition of DNA. The I response was calculated by averaging the raw source–drain current data over each period of the liquid gate triangle wave. I response signals are shown here as percentage changes. The C response is the percentage change in the slope of the gFET transfer curve relative to a calibration step and was calculated for each gate loop from the raw source–drain current data. Changes in the C response are probably dominated by changes in the capacitance between the graphene channel and the liquid as material binds to the surface. The detailed method for calculating C responses is described in the Supplementary Information. V response values were calculated by dividing the current by the transconductance in a linear region of the transfer curve. Following our previous work describing the device physics of these sensors[66], this value is presented as the percentage difference relative to the calibration step. The detailed method for calculating the V response is described in the Supplementary Information. This value is like the Dirac voltage shift or, more generally, a transistor threshold voltage shift, but is a calculated value rather than a measured value and should not be taken to imply an actual voltage measurement on the surface.

Agile Plus software (Cardea) was used to run the Agile R100 reader system. Approximately 10% of transistors failed during measurement due to one or more graphene channels open circuiting. The software detected these failures as instantaneous drops of 15% or more in the source–drain current. The remaining 90% of devices measured were analysed using Python scripts and KNIME workflows to calculate capacitance and effective gate potential data. The statistics were calculated using Prism, assuming a normal distribution of the data.

Reproducibility of the SNP-Chip studies. The SNP-Chip studies were performed by two researchers to ensure the reproducibility of the results. It is clear from all of the sensing data presented in this paper that assuming a normal distribution results in a calculated error that is larger than the true variations in the sensing signals. Some variations present in the sensing data are recognizable across multiple datasets. One potential source of variation is the biofunctionalization (that is, the immobilization of Cas9 and gRNA on the surface of the gFET). We have provided data (Supplementary Fig. 5) that characterize the variation in immobilization signal of both Cas9 and gRNA. This implies that future research could produce calibration or process techniques that could improve the statistics of the overall measurement system. We show one approach to addressing this here: increasing the specificity of the core biochemical system. This opens promising areas for future studies to enhance sensor sensitivity further.

Reporting Summary. Further information on research design is available in the Nature Research Reporting Summary linked to this article.

Data availability

The main data supporting the results in this study are available within the paper and its Supplementary Information. All data generated in this study, including source data used to make the figures, are available from Figshare (https://doi.org/10.6084/m9.figshare.14067230). Raw electronic datasets generated during the study are too large (7.743 GB) to be shared publicly but are available for research purposes from the corresponding author upon reasonable request.

Code availability

The software used for analysis is available for research purposes from the corresponding author upon reasonable request. A licence for use of this software would need to be obtained from Cardea.

Received: 11 July 2020; Accepted: 23 February 2021;
Published online: 5 April 2021

References

1. Rees, H. A. & Liu, D. R. Base editing: precision chemistry on the genome and transcriptome of living cells. *Nat. Rev. Genet.* **19**, 770–788 (2018).
2. Landrum, M. J. et al. ClinVar: public archive of relationships among sequence variation and human phenotype. *Nucleic Acids Res.* **42**, D980–D985 (2013).
3. Landrum, M. J. et al. ClinVar: public archive of interpretations of clinically relevant variants. *Nucleic Acids Res.* **44**, D862–D868 (2015).
4. Hawn, T. R. et al. Toll-like receptor polymorphisms and susceptibility to urinary tract infections in adult women. *PLoS ONE* **4**, e5990 (2009).
5. Johnson, C. M. et al. Cutting edge: a common polymorphism impairs cell surface trafficking and functional responses of TLR1 but protects against leprosy. *J. Immunol.* **178**, 7520–7524 (2007).
6. Sironi, M. et al. A common polymorphism in *TLR3* confers natural resistance to HIV-1 infection. *J. Immunol.* **188**, 818–823 (2012).
7. Pagliai, G. et al. *CLOCK* gene polymorphisms and quality of aging in a cohort of nonagenarians—The MUGELLO Study. *Sci. Rep.* **9**, 1472 (2019).
8. Yang, C.-H., Cheng, Y.-H., Chuang, L.-Y. & Chang, H.-W. Drug-SNPing: an integrated drug-based, protein interaction-based tagSNP-based pharmacogenomics platform for SNP genotyping. *Bioinformatics* **29**, 758–764 (2013).
9. Alwi, Z. B. The use of SNPs in pharmacogenomics studies. *Malays. J. Med. Sci.* **12**, 4–12 (2005).
10. McCarthy, J. J. & Hilfiker, R. The use of single-nucleotide polymorphism maps in pharmacogenomics. *Nat. Biotechnol.* **18**, 505–508 (2000).
11. Chagné, D. et al. Validation of SNP markers for fruit quality and disease resistance loci in apple (*Malus* × *domestica* Borkh.) using the OpenArray® platform. *Horticulture Res.* **6**, 30 (2019).
12. Kennedy, R. B. et al. Genetic polymorphisms associated with rubella virus-specific cellular immunity following MMR vaccination. *Hum. Genet.* **133**, 1407–1417 (2014).
13. Dhiman, N. et al. SNP/haplotype associations in cytokine and cytokine receptor genes and immunity to rubella vaccine. *Immunogenetics* **62**, 197–210 (2010).
14. He, J. et al. Association of SARS susceptibility with single nucleic acid polymorphisms of *OAS1* and *MxA* genes: a case-control study. *BMC Infect. Dis.* **6**, 106 (2006).
15. Gralinski, L. E. et al. Genome wide identification of SARS-CoV susceptibility loci using the collaborative cross. *PLoS Genet.* **11**, e1005504 (2015).
16. Itoyama, S. et al. ACE1 polymorphism and progression of SARS. *Biochem. Biophys. Res. Commun.* **323**, 1124–1129 (2004).
17. Guan, Y. et al. Isolation and characterization of viruses related to the SARS coronavirus from animals in Southern China. *Science* **302**, 276–278 (2003).
18. Kan, B. et al. Molecular evolution analysis and geographic investigation of severe acute respiratory syndrome coronavirus-like virus in palm civets at an animal market and on farms. *J. Virol.* **79**, 11892–11900 (2005).
19. Gisler, F. M., von Kanel, T., Kraemer, R., Schaller, A. & Gallati, S. Identification of SNPs in the cystic fibrosis interactome influencing pulmonary progression in cystic fibrosis. *Eur. J. Hum. Genet.* **21**, 397–403 (2013).
20. Williams, L. M. & Oleksiak, M. F. Ecologically and evolutionarily important SNPs identified in natural populations. *Mol. Biol. Evol.* **28**, 1817–1826 (2011).
21. López-García, M. A. et al. Influence of genetic variants of CYP2D6, CYP2C9, CYP2C19 and CYP3A4 on antiepileptic drug metabolism in pediatric patients with refractory epilepsy. *Pharmacol. Rep.* **69**, 504–511 (2017).
22. Barilli, E. et al. A high-density integrated DArTseq SNP-based genetic map of *Pisum fulvum* and identification of QTLs controlling rust resistance. *Front. Plant Sci.* **9**, 167 (2018).
23. Zhang, T. et al. Identification of molecular markers associated with verticillium wilt resistance in alfalfa (*Medicago Sativa* L.) using high-resolution melting. *PLoS ONE* **9**, e115953 (2014).
24. Rey, T. et al. The Medicago truncatula GRAS protein RAD1 supports arbuscular mycorrhiza symbiosis and *Phytophthora palmivora* susceptibility. *J. Exp. Bot.* **68**, 5871–5881 (2017).
25. Ben Ali, S.-E. et al. Mutation scanning in a single and a stacked genetically modified (GM) event by real-time PCR and high resolution melting (HRM) analysis. *Int. J. Mol. Sci.* **15**, 19898–19923 (2014).
26. Gunderson, K. L., Steemers, F. J., Lee, G., Mendoza, L. G. & Chee, M. S. A genome-wide scalable SNP genotyping assay using microarray technology. *Nat. Genet.* **37**, 549–554 (2005).
27. Yamamoto, G. et al. Highly sensitive method for genomewide detection of allelic composition in nonpaired, primary tumor specimens by use of affymetrix single-nucleotide-polymorphism genotyping microarrays. *Am. J. Hum. Genet.* **81**, 114–126 (2007).
28. Gaedigk, A. et al. SNP genotyping using TaqMan® technology: the *CYP2D6*17* assay conundrum. *Sci. Rep.* **5**, 9257 (2015).
29. Borodina, T. A., Lehrach, H. & Soldatov, A. V. Ligation detection reaction-TaqMan procedure for single nucleotide polymorphism detection on genomic DNA. *Anal. Biochem.* **333**, 309–319 (2004).

30. Ramos, A. M. et al. Design of a high density SNP genotyping assay in the pig using SNPs identified and characterized by next generation sequencing technology. *PLoS ONE* **4**, e6524 (2009).
31. Hajian, R. et al. Detection of unamplified target genes via CRISPR–Cas9 immobilized on a graphene field-effect transistor. *Nat. Biomed. Eng.* **3**, 427–437 (2019).
32. Boyle, E. A. et al. High-throughput biochemical profiling reveals sequence determinants of dCas9 off-target binding and unbinding. *Proc. Natl Acad. Sci. USA* **114**, 5461–5466 (2017).
33. Anders, C., Niewoehner, O., Duerst, A. & Jinek, M. Structural basis of PAM-dependent target DNA recognition by the Cas9 endonuclease. *Nature* **513**, 569–573 (2014).
34. Josephs, E. A. et al. Structure and specificity of the RNA-guided endonuclease Cas9 during DNA interrogation, target binding and cleavage. *Nucleic Acids Res.* **43**, 8924–8941 (2015).
35. Pattanayak, V. et al. High-throughput profiling of off-target DNA cleavage reveals RNA-programmed Cas9 nuclease specificity. *Nat. Biotechnol.* **31**, 839–843 (2013).
36. Qi, L. S. et al. Repurposing CRISPR as an RNA-guided platform for sequence-specific control of gene expression. *Cell* **152**, 1173–1183 (2013).
37. Zhao, C., Shu, X. & Sun, B. Construction of a gene knockdown system based on catalytically inactive ("dead") Cas9 (dCas9) in *Staphylococcus aureus*. *Appl. Environ. Microbiol.* **83**, e00291-17 (2017).
38. Sternberg, S. H., Redding, S., Jinek, M., Greene, E. C. & Doudna, J. A. DNA interrogation by the CRISPR RNA-guided endonuclease Cas9. *Nature* **507**, 62–67 (2014).
39. Chatterjee, P., Jakimo, N. & Jacobson, J. M.Minimal PAM specificity of a highly similar SpCas9 ortholog. *Sci. Adv.* **4**, eaau0766 (2018).
40. Chen, J. S. et al. Enhanced proofreading governs CRISPR–Cas9 targeting accuracy. *Nature* **550**, 407–410 (2017).
41. Kleinstiver, B. P. et al. High-fidelity CRISPR–Cas9 variants with undetectable genome-wide off-targets. *Nature* **529**, 490–495 (2016).
42. Slaymaker, I. M. et al. Rationally engineered Cas9 nucleases with improved specificity. *Science* **351**, 84–88 (2016).
43. Zhang, D. et al. Perfectly matched 20-nucleotide guide RNA sequences enable robust genome editing using high-fidelity SpCas9 nucleases. *Genome Biol.* **18**, 191 (2017).
44. Vakulskas, C. A. et al. A high-fidelity Cas9 mutant delivered as a ribonucleoprotein complex enables efficient gene editing in human hematopoietic stem and progenitor cells. *Nat. Med.* **24**, 1216–1224 (2018).
45. Cai, L. et al. A universal approach to correct various *HBB* gene mutations in human stem cells for gene therapy of beta-thalassemia and sickle cell disease. *Stem Cells Transl. Med.* **7**, 87–97 (2017).
46. Eaton, W. A. Hemoglobin S polymerization and sickle cell disease: a retrospective on the occasion of the 70th anniversary of Pauling's *Science* paper. *Am. J. Hematol.* **95**, 205–211 (2020).
47. Papageorgiou, D. P. et al. Simultaneous polymerization and adhesion under hypoxia in sickle cell disease. *Proc. Natl Acad. Sci. USA* **115**, 9473–9478 (2018).
48. Sachdev, V., Rosing, D. R. & Thein, S. L. Cardiovascular complications of sickle cell disease. *Trends Cardiovasc. Med.* https://doi.org/10.1016/j.tcm.2020.02.002 (2020).
49. Piel, F. B., Steinberg, M. H. & Rees, D. C. Sickle cell disease. *N. Engl. J. Med.* **376**, 1561–1573 (2017).
50. Quinn, C. T., Rogers, Z. R., McCavit, T. L. & Buchanan, G. R.Improved survival of children and adolescents with sickle cell disease. *Blood* **115**, 3447–3452 (2010).
51. Gong, L., Parikh, S., Rosenthal, P. J. & Greenhouse, B. Biochemical and immunological mechanisms by which sickle cell trait protects against malaria. *Malar. J.* **12**, 317 (2013).
52. Robberecht, W. & Philips, T. The changing scene of amyotrophic lateral sclerosis. *Nat. Rev. Neurosci.* **14**, 248–264 (2013).
53. Al-Chalabi, A. et al. The genetics and neuropathology of amyotrophic lateral sclerosis. *Acta Neuropathol.* **124**, 339–352 (2012).
54. Borchelt, D. R. et al. Superoxide dismutase 1 with mutations linked to familial amyotrophic lateral sclerosis possesses significant activity. *Proc. Natl Acad. Sci. USA* **91**, 8292–8296 (1994).
55. Nordlund, A. et al. Functional features cause misfolding of the ALS-provoking enzyme SOD1. *Proc. Natl Acad. Sci. USA* **106**, 9667–9672 (2009).
56. Pattabhi, S. et al. In vivo outcome of homology-directed repair at the *HBB* gene in HSC using alternative donor template delivery methods. *Mol. Ther. Nucleic Acids* **17**, 277–288 (2019).
57. Dever, D. P. et al. CRISPR/Cas9 β-globin gene targeting in human hematopoietic stem cells. *Nature* **539**, 384–389 (2016).
58. Park, S. H. et al. Highly efficient editing of the β-globin gene in patient-derived hematopoietic stem and progenitor cells to treat sickle cell disease. *Nucleic Acids Res.* **47**, 7955–7972 (2019).
59. Duan, W. et al. The deletion of mutant SOD1 via CRISPR/Cas9/sgRNA prolongs survival in an amyotrophic lateral sclerosis mouse model. *Gene Ther.* **27**, 157–169 (2020).
60. Gaj, T. et al. In vivo genome editing improves motor function and extends survival in a mouse model of ALS. *Sci. Adv.* **3**, eaar3952 (2017).
61. Aryal, N. K., Wasylishen, A. R. & Lozano, G. CRISPR/Cas9 can mediate high-efficiency off-target mutations in mice in vivo. *Cell Death Dis.* **9**, 1099 (2018).
62. Cho, S. W. et al. Analysis of off-target effects of CRISPR/Cas-derived RNA-guided endonucleases and nickases. *Genome Res.* **24**, 132–141 (2014).
63. DeWitt, M. A. et al. Selection-free genome editing of the sickle mutation in human adult hematopoietic stem/progenitor cells. *Sci. Transl. Med.* **8**, 360ra134 (2016).
64. Bowden, R. et al. Sequencing of human genomes with nanopore technology. *Nat. Commun.* **10**, 1869 (2019).
65. Hwang, M. T. et al. Highly specific SNP detection using 2D graphene electronics and DNA strand displacement. *Proc. Natl Acad. Sci. USA* **113**, 7088–7093 (2016).
66. Goldsmith, B. R. et al. Digital biosensing by foundry-fabricated graphene sensors. *Sci. Rep.* **9**, 434 (2019).
67. Afsahi, S. et al. Novel graphene-based biosensor for early detection of Zika virus infection. *Biosens. Bioelectron.* **100**, 85–88 (2018).
68. Sadlowski, C. et al. Graphene-based biosensor for on-chip detection of bio-orthogonally labeled proteins to identify the circulating biomarkers of aging during heterochronic parabiosis. *Lab Chip* **18**, 3230–3238 (2018).
69. Wickramathilaka, M. P. & Tao, B. Y. Characterization of covalent crosslinking strategies for synthesizing DNA-based bioconjugates. *J. Biol. Eng.* **13**, 63 (2019).
70. Riquelme, M. V. et al. Optimizing blocking of nonspecific bacterial attachment to impedimetric biosensors. *Sens. Biosensing Res.* **8**, 47–54 (2016).
71. Singh, D., Sternberg, S. H., Fei, J., Doudna, J. A. & Ha, T. Real-time observation of DNA recognition and rejection by the RNA-guided endonuclease Cas9. *Nat. Commun.* **7**, 12778 (2016).
72. Knight, S. C. et al. Dynamics of CRISPR–Cas9 genome interrogation in living cells. *Science* **350**, 823–826 (2015).
73. Yang, M. et al. The conformational dynamics of Cas9 governing DNA cleavage are revealed by single-molecule FRET. *Cell Rep.* **22**, 372–382 (2018).
74. Jinek, M. et al. A programmable dual RNA-guided DNA endonuclease in adaptive bacterial immunity. *Science* **337**, 816–821 (2012).
75. Bialk, P. et al. Analyses of point mutation repair and allelic heterogeneity generated by CRISPR/Cas9 and single-stranded DNA oligonucleotides. *Sci. Rep.* **6**, 32681 (2016).
76. Daer, R. M., Cutts, J. P., Brafman, D. A. & Haynes, K. A. The impact of chromatin dynamics on Cas9-mediated genome editing in human cells. *ACS Synth. Biol.* **6**, 428–438 (2017).
77. Amrani, N. et al. NmeCas9 is an intrinsically high-fidelity genome-editing platform. *Genome Biol.* **19**, 214 (2018).
78. Harrington, L. B. et al. A thermostable Cas9 with increased lifetime in human plasma. *Nat. Commun.* **8**, 1424 (2017).
79. Hu, Z. et al. A compact Cas9 ortholog from *Staphylococcus auricularis* (SauriCas9) expands the DNA targeting scope. *PLoS Biol.* **18**, e3000686 (2020).
80. D'Agata, R. et al. Direct detection of point mutations in nonamplified human genomic DNA. *Anal. Chem.* **83**, 8711–8717 (2011).
81. Rosen, D. R. et al. Mutations in Cu/Zn superoxide dismutase gene are associated with familial amyotrophic lateral sclerosis. *Nature* **362**, 59–62 (1993).
82. Cong, L. et al. Multiplex genome engineering using CRISPR/Cas systems. *Science* **339**, 819–823 (2013).
83. Ran, F. A. et al. Genome engineering using the CRISPR–Cas9 system. *Nat. Protoc.* **8**, 2281–2308 (2013).
84. Yang, Z., Edwards, H. & Xu, P. CRISPR–Cas12a/Cpf1-assisted precise, efficient and multiplexed genome-editing in *Yarrowia lipolytica*. *Metab. Eng. Commun.* **10**, e00112 (2020).
85. Abudayyeh, O. O. et al. C2c2 is a single-component programmable RNA-guided RNA-targeting CRISPR effector. *Science* **353**, aaf5573 (2016).
86. Gootenberg, J. S. et al. Nucleic acid detection with CRISPR–Cas13a/C2c2. *Science* **356**, 438–442 (2017).
87. Gasiunas, G., Barrangou, R., Horvath, P. & Siksnys, V. Cas9–crRNA ribonucleoprotein complex mediates specific DNA cleavage for adaptive immunity in bacteria. *Proc. Natl Acad. Sci. USA* **109**, E2579 (2012).
88. Gasiunas, G. et al. A catalogue of biochemically diverse CRISPR–Cas9 orthologs. *Nat. Commun.* **11**, 5512 (2020).
89. Povedano, E. et al. Electrochemical affinity biosensors for fast detection of gene-specific methylations with no need for bisulfite and amplification treatments. *Sci. Rep.* **8**, 6418 (2018).
90. Rauf, S. et al. Carboxylic group riched graphene oxide based disposable electrochemical immunosensor for cancer biomarker detection. *Anal. Biochem.* **545**, 13–19 (2018).

91. Guo, L. et al. Colorimetric biosensor for the assay of paraoxon in environmental water samples based on the iodine-starch color reaction. *Anal. Chim. Acta* **967**, 59–63 (2017).
92. Lang, Q., Han, L., Hou, C., Wang, F. & Liu, A. A sensitive acetylcholinesterase biosensor based on gold nanorods modified electrode for detection of organophosphate pesticide. *Talanta* **156–157**, 34–41 (2016).
93. Greig, D. R., Jenkins, C., Gharbia, S. & Dallman, T. J.Comparison of single-nucleotide variants identified by Illumina and Oxford Nanopore technologies in the context of a potential outbreak of Shiga toxin-producing *Escherichia coli*. *GigaScience* **8**, giz104 (2019).
94. Caputo, T. M., Battista, E., Netti, P. A. & Causa, F. Supramolecular microgels with molecular beacons at the interface for ultrasensitive, amplification-free, and SNP-selective miRNA fluorescence detection. *ACS Appl. Mater. Interfaces* **11**, 17147–17156 (2019).
95. Yang, Z. et al. An amplification-free detection method of nucleic acids by a molecular beacon probe based on endonuclease activity. *Sens. Actuators B* **298**, 126901 (2019).
96. Gilpatrick, T. et al. Targeted nanopore sequencing with Cas9-guided adapter ligation. *Nat. Biotechnol.* **38**, 433–438 (2020).
97. Walton, R. T., Christie, K. A., Whittaker, M. N. & Kleinstiver, B. P.Unconstrained genome targeting with near-PAMless engineered CRISPR–Cas9 variants. *Science* **368**, 290–296 (2020).
98. Everaerts, F., Torrianni, M., Hendriks, M. & Feijen, J. Biomechanical properties of carbodiimidecrosslinked collagen: influence of the formation of ester crosslinks. *J Biomed Mater Res A* **85**, 547–555 (2008).
99. Wang, C., Yan, Q., Liu, H.-B., Zhou, X.-H. & Xiao, S.-J. Different EDC/NHS Activation Mechanismsbetween PAA and PMAA Brushes and the Following Amidation Reactions. *Langmuir* **27**, 12058–12068 (2011).

Acknowledgements

We acknowledge H. Aldaz and K. Forster for contributions towards manuscript preparation. The schematics in Figs. 2a,e, 3a,b,f, 4e and 5f and Supplementary Figs. 3a and 5a,c were created with BioRender.com. This work was primarily supported by Cardea-sponsored research awarded to the Aran laboratory, with additional support from NSF award 2048283 and the Open Philanthropy award to I.M.C. Support for J.J.T. was from NSF INTERN award 1827671.

Author contributions

K.A. designed and developed the technology with initial assistance from I.M.C. R.H. performed the initial optimization studies for Cas immobilization on graphene. J.J.T. performed the AFM studies and data analysis, with assistance with sample preparation from R.H. and supervision from P.G.C. S.B. optimized the SNP-Chip design with assistance from K.F. and supervision from K.A. S.B. performed the SNP-Chip amplicon experiments with assistance from K.F. and supervision from K.A. S.B. performed the genomic DNA experiments with the dCas9, Cas9 and MgaCas9 SNP-Chip constructs, with assistance with sample preparation and data acquisition from E.C, A.J. and K.D., and supervision from K.A. R.P. assisted with SNP-Chip assay optimization. J.J.T. and S.B. performed data analysis, with assistance from J.P. and supervision from P.G.C and K.A. S.K. purified MgaCas9 and assisted with gRNA synthesis and validation. G.G. performed an in vitro cleavage assay for the MgaCas9 complexes. D.K. participated in the planning and execution of the experiments in Fig. 4. F.B. and B.R.G. assisted with gFET production. V.S. assisted with experimental design. S.B. and K.A. prepared the manuscript with assistance from J.J.T., E.C., K.F., K.S., G.G., K.D., J.J.R., H.L., F.B., B.R.G., P.G.C., I.M.C. and V.S.

Competing interests

K.A. is a co-founder of Cardea. V. S. is a co-founder of CasZyme. The remaining authors declare no competing interests.

Additional information

Supplementary information The online version contains supplementary material available at https://doi.org/10.1038/s41551-021-00706-z.

Correspondence and requests for materials should be addressed to K.A.

Peer review information *Nature Biomedical Engineering* thanks Jonathan Gootenberg and the other, anonymous, reviewer(s) for their contribution to the peer review of this work. Peer reviewer reports are available.

Reprints and permissions information is available at www.nature.com/reprints.

Publisher's note Springer Nature remains neutral with regard to jurisdictional claims in published maps and institutional affiliations.

nature research

Corresponding author(s): Kiana Aran

Last updated by author(s): Feb 21, 2021

Reporting Summary

Nature Research wishes to improve the reproducibility of the work that we publish. This form provides structure for consistency and transparency in reporting. For further information on Nature Research policies, see our Editorial Policies and the Editorial Policy Checklist.

Statistics

For all statistical analyses, confirm that the following items are present in the figure legend, table legend, main text, or Methods section.

n/a	Confirmed	
☐	☒	The exact sample size (*n*) for each experimental group/condition, given as a discrete number and unit of measurement
☐	☒	A statement on whether measurements were taken from distinct samples or whether the same sample was measured repeatedly
☐	☒	The statistical test(s) used AND whether they are one- or two-sided *Only common tests should be described solely by name; describe more complex techniques in the Methods section.*
☒	☐	A description of all covariates tested
☐	☒	A description of any assumptions or corrections, such as tests of normality and adjustment for multiple comparisons
☐	☒	A full description of the statistical parameters including central tendency (e.g. means) or other basic estimates (e.g. regression coefficient) AND variation (e.g. standard deviation) or associated estimates of uncertainty (e.g. confidence intervals)
☐	☒	For null hypothesis testing, the test statistic (e.g. *F*, *t*, *r*) with confidence intervals, effect sizes, degrees of freedom and *P* value noted *Give P values as exact values whenever suitable.*
☒	☐	For Bayesian analysis, information on the choice of priors and Markov chain Monte Carlo settings
☒	☐	For hierarchical and complex designs, identification of the appropriate level for tests and full reporting of outcomes
☒	☐	Estimates of effect sizes (e.g. Cohen's *d*, Pearson's *r*), indicating how they were calculated

Our web collection on statistics for biologists contains articles on many of the points above.

Software and code

Policy information about availability of computer code

Data collection	Agile Plus software was used to run the Agile R100 reader system (Cardea, San Diego, CA).
Data analysis	The Anaconda distribution of python was used in conjuntion with the Knime data-analysis environment to analyse the data.

For manuscripts utilizing custom algorithms or software that are central to the research but not yet described in published literature, software must be made available to editors and reviewers. We strongly encourage code deposition in a community repository (e.g. GitHub). See the Nature Research guidelines for submitting code & software for further information.

Data

Policy information about availability of data

All manuscripts must include a data availability statement. This statement should provide the following information, where applicable:

- Accession codes, unique identifiers, or web links for publicly available datasets
- A list of figures that have associated raw data
- A description of any restrictions on data availability

The main data supporting the results in this study are available within the paper and its Supplementary Information. All data generated in this study, including source data used to make the figures, are available from figshare with the identifier 10.6084/m9.figshare.14067230. Raw electronic datasets generated during the study are too large (7.743 GB) to be publicly shared, yet they are available for research purposes from the corresponding author on reasonable request.

Field-specific reporting

Please select the one below that is the best fit for your research. If you are not sure, read the appropriate sections before making your selection.

☒ Life sciences ☐ Behavioural & social sciences ☐ Ecological, evolutionary & environmental sciences

For a reference copy of the document with all sections, see nature.com/documents/nr-reporting-summary-flat.pdf

Life sciences study design

All studies must disclose on these points even when the disclosure is negative.

Sample size	Sample sizes were subject to sample availability. For the majority of the studies, three or more chips were used (each chip had at least two functional transistors) to ensure reproducibility. For the blind studies, there were three patients per cohort and one chip per patient was used (with each cheap having at least two functional transistors).
Data exclusions	Around ~10% of the transistors failed owing to a break in the electrical connection during measurement. The software is designed to detect these failures and to remove those transistors when they break.
Replication	The SNP-Chip studies were performed by two researchers to ensure the reproducibility of the results. For the majority of the studies three or more chips were used, to ensure reproducibility. For the blind studies, three patients per cohort and one chip per patient were used (with each chip having at least two functional transistors).
Randomization	The samples were not randomized. SCD samples, samples from healthy individuals, and heterozygous samples were classified as such on the basis of informations provided by the commercial vendor.
Blinding	The investigators were blinded to group allocation during sample collection and analysis for the studies presented in Fig. 5. All other studies were not carried out in a blind manner.

Reporting for specific materials, systems and methods

We require information from authors about some types of materials, experimental systems and methods used in many studies. Here, indicate whether each material, system or method listed is relevant to your study. If you are not sure if a list item applies to your research, read the appropriate section before selecting a response.

Materials & experimental systems

n/a	Involved in the study
☒	☐ Antibodies
☐	☒ Eukaryotic cell lines
☒	☐ Palaeontology and archaeology
☒	☐ Animals and other organisms
☐	☒ Human research participants
☒	☐ Clinical data
☒	☐ Dual use research of concern

Methods

n/a	Involved in the study
☒	☐ ChIP-seq
☒	☐ Flow cytometry
☒	☐ MRI-based neuroimaging

Eukaryotic cell lines

Policy information about cell lines

Cell line source(s)	An induced pluripotent stem cell line from an human ALS patient fibroblast (Latino, female, 35 years old). The original cell line name from Cedars-Sinai is CS04iALS-SOD1H44Rnxx.
Authentication	We purchased this cell line from the induced pluripotent stem cell core in Cedars-Sinai (Los Angeles, CA).
Mycoplasma contamination	We regularly checked for mycoplasma contamination. No contamination was found.
Commonly misidentified lines (See ICLAC register)	No commonly misidentified cell lines were used.

Human research participants

Policy information about studies involving human research participants

Population characteristics	NA03798 corresponds to an apparently healthy 10-year-old male. NA22807 corresponds to an apparently healthy 52-year-old male.

NA23904 corresponds to an apparently healthy 65-year-old male.
NA16265 corresponds to a 19-year-old male with sickle cell anemia homozygous for an A-to-T transversion (GAG>GTG) at nucleotide 20 in exon 1 of the HBB gene, which results in the substitution of valine for glutamic acid [GLU6VAL (E6V)] at codon 6; the genotype is homozygous Hb S (HbSS).
NA16267 corresponds to a 3-year-old male who has sickle cell disease and beta-plus-thalassemia; two copies of the following mutation were identified: an A-to-T transversion (GAG>GTG) at nucleotide 20 in exon 1 of the HBB gene, which results in the substitution of valine for glutamic acid [GLU6VAL (E6V)] at codon 6; the beta-plus-thalassemia mutation is not known.
NA16266 corresponds to a male of unknown age with hemoglobin SC disease; the donor subject is a compound heterozygote; one allele carries a G-to-A transition (GAG>AAG) in the HBB gene, which results in the substitution of lysine for glutamic acid [GLU6LYS (E6K)] at codon 6; the second allele has an A-to-T transversion (GAG>GTG) at nucleotide 20 in exon 1 of the HBB gene, which results in the substitution of valine for glutamic acid [GLU6VAL (E6V)] at codon 6; the genotype is Hb SC.
NA20838 corresponds to a 35-year-old African American female clinically healthy; sickle cell trait; 2–3 episodes of epistaxis per week from age 8 to 11 years; type-II diabetes diagnosed in adulthood; haemoglobin electrophoresis results: HbA = 61.4%, HbA2 = 3.8%, HbF = 0%, HbS = 34.8%; hemoglobin = 11.1 g/dl; MCV = 77.2.

Recruitment

Human samples were purchased from a commercial vendor (Corriell Institute).

Ethics oversight

Not applicable because samples were purchased from a commercial vendor (Corriell Institute).

Note that full information on the approval of the study protocol must also be provided in the manuscript.